OPTICAL CHARACTERIZATION OF A HIGH SPEED PLASMA'S ELECTROMAGNETIC PROPERTIES

A Thesis
Presented to
The Academic Faculty

By

Parker Singletary

In Partial Fulfillment
of the Requirements for the Degree
Master's of Science in the
School of Electrical and Computer Engineering

Georgia Institute of Technology

May 2018

OPTICAL CHARACTERIZATION OF A HIGH SPEED PLASMA'S ELECTROMAGNETIC PROPERTIES

Approved by:

Dr. Morris Cohen, Advisor
School of Electrical and Computer Engineering
Georgia Institute of Technology

Dr. Thomas Gaylord
School of Electrical and Computer Engineering
Georgia Institute of Technology

Dr. Mitchell Walker
School of Aerospace Engineering
Georgia Institute of Technology

Dr. Sven Simon
School of Earth and Atmospheric Sciences
Georgia Institute of Technology

Date Approved: April 16, 2018

To my parents, Ruth and Ted.

ACKNOWLEDGEMENTS

First and foremost, I would like to thank my advisor, Dr. Morris Cohen, for offering me a position in the LF research lab. Coming to graduate school and starting research is a daunting task, but Dr. Cohen's advice and patience has made this process enjoyable and fulfilling. It is truly a privilege to be one of his students.

A tremendous thank you to Dr. Thomas Gaylord, Dr. Mitchell Walker, and Dr. Sven Simon for serving on my thesis advising committee. A professor's job is not easy, and thesis review is time consuming. Their willingness to take to time to read my work is appreciated beyond words.

I would like to thank the members of the LF lab for their help through these years: Nick Gross, Jackson McCormick, Marc Higginson-Rollins, and Nathan Opalinski. The encouragement they all have given me, and the innumerable code errors they have helped me diagnose has helped me keep my sanity.

This research would not have been possible without the support of members of the HPEPL. Cheong Chan was instrumental in designing the original plasma chamber. Connie Liu, Rob Ashcom, and Divya Sunkara spent countless hours this semester designing, building, and re-configuring our test bed. Even more of their time was spent recording and processing data. I can't thank them enough.

I certainly would not be here today without my family. They raised me through the years and helped me grow into the person I am today. I owe my success to them.

Finally, I would like to thank my fiancée (wife once June 2nd rolls around) Annsley. Her motivation and love through this research and writing process has kept me going through times when I wanted to give up and go drive trains for a living. I look forward spending the rest of my days with you, and going through this process with you again when it's time to write my dissertation!

TABLE OF CONTENTS

LIST OF TABLES

LIST OF FIGURES

SUMMARY

Very Low Frequency (VLF, 3-30kHz) and Low Frequency (LF, 30-300kHz) radio waves are useful due to their ability to travel around the world in the Earth-Ionosphere waveguide and excellent skin depth penetration into conductors. However, generation of these waves is limited due to the fact that their wavelengths are hundreds of meters to kilometers long. A recently proposed antenna concept known as VAIPER involves an antenna with time-varying conductivity. The antenna's properties need to be varied at nanosecond timescales. This time-varying concept can be realized at low power with COTS components, but high speed switches cannot handle high power. A plasma is a conducting media with electrical properties that can be varied rapidly while handling high current flow. Antennas made from plasma have been constructed and tested in the past, but not with rapidly time-varying conductivity in mind. To determine a plasma's viability as an antenna, its electromagnetic properties must be measured. Conventional plasma analysis techniques do not resolve variations in plasma at the desired speeds. The objective of the research in this thesis is to develop techniques to analyze a plasma column's electric properties as it is ionized and de-ionized on the nanosecond timescales. Optical techniques are used to determine the time-varying conductivity of rapidly pulsed plasma. The conductivity measurements fed into a basic propagation model to determine whether the experimental plasma columns can support the VAIPER scheme.

CHAPTER 1
INTRODUCTION AND BACKGROUND

1.1 VLF and LF Electromagnetic Waves

Very Low Frequency (VLF, 3-30 kHz) and Low Frequency (LF, 30-300 kHz) waves have the ability to travel around the world with low loss, guided by reflections from the D-region of the ionosphere ($60-90$ km altitude) and the Earth, which form a waveguide. Waves at these frequencies also penetrate seawater via the skin effect, allowing signals to be received by submerged submarines. Additionally, they propagate deep into the ground and can be used for subterranean sensing. Although VLF and LF waves are quite useful, these longwave frequencies are exceedingly difficult to generate efficiently due to their long wavelengths (1-100 km). Efficient radio antennas are often comparable to their operating frequencys wavelength in size, such as a half-wave dipole. For higher frequency (UHF, SHF) applications such as consumer electronics, antenna size isn't a limitation because wavelengths are typically less than a meter long. For VLF/LF frequencies, building an antenna comparable to the operating wavelength difficult. The US Navy as well as others have generated these frequencies successfully utilizing heavily engineered electrically short antennas, with length far less than the operating wavelength. Electrically short antennas have highly reactive input impedances due to the reflection of the signal at the end of the antenna. The fundamental reason for this is that at low frequencies, in the time it takes voltage to travel down, reflect, and arrive at the antenna feed, the feed current has barely changed, so the reflected current virtually cancels out the feed current while the voltage adds up. The effects of this reflection can be dealt with via top loading, which is described in depth in [1]. This frequency-domain matching technique introduces a resonance to the antenna, so it only operates efficiently in a narrow range of frequencies. An example of

a pair US Navy VLF antennas is located in Cutler, Maine, transmitting 1 MW at 24 kHz, corresponding to a wavelength of 12.5 kilometers. These antennas are shown in Figure 1.1. The top hat of one of the Cutler antennas is 1.87 km in diameter, requiring a large footprint. The sheer size of one of these top loaded antennas make them difficult to maintain and effectively impossible to transport.

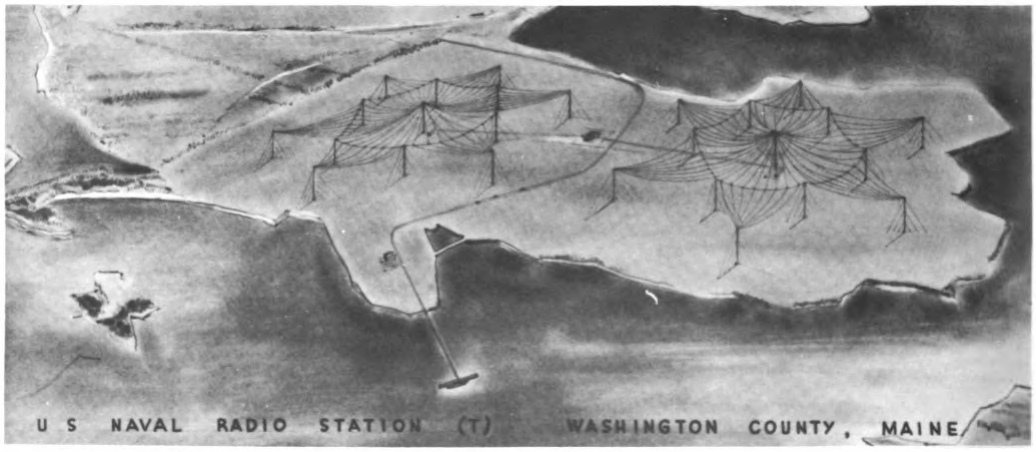

Figure 1.1: VLF transmitter NAA at Cutler, Maine [1].

The bandwidth of existing US Navy transmitters is $\sim$200 Hz. Changing the operating frequency also requires a redesign and overhaul of the array as its components are designed and tuned specifically for its operating range. A portable and more adaptable VLF transmitter with a wider bandwidth is highly desirable. A new concept was recently proposed [2] to generate LF waves with electrically short antennas via time-domain reflection suppression in lieu of frequency-domain matching techniques. Rather than feeding the antenna with a pure sinusoid, it is fed with a series of extremely short ($<$10 ns) voltage pulses with peaks that follow the envelope of the sinusoid. As each pulse reaches the tip of the antenna, the antenna's conductivity is lowered at a point close to the tip, attenuating the pulse and eliminating the reflection. Therefore, the charge is deposited at the tip, and the returning current does not flow back to cancel out the injected current. Because this matching technique is done in the time domain, in principle it works at frequency, leading to full broadband

capability. The lack of need for a top hat enables an antenna built as such to be potentially portable. Some efficiency is lost when a sinusoidal signal is converted into a train of pulses. To mitigate this effect, the pulses should be as close to one another in time as possible to maximize efficiency. At the same time, the pulses must be shorter than the propagation delay from the antenna's feed to its tip. If the antenna is 3 meters long, and propagation is at the speed of light, the pulse duration must be noticeably less than 10 ns. During the 10 ns period, the antenna must be highly conductive to allow high power pulses. This concept can be realized using high speed switching electronics, but those electrical components cannot handle the high power needed for long range transmission. As such, the focus of this thesis is using a rapidly pulsed, segmented plasma column in lieu of electronics. The length and frequency of pulses will be limited by the plasma's ionization time, de-ionization time, and conductivity. Our aim is to define the methodology to measure pulsed plasma column's parameters and compare these to benchmarks that we will establish: fast rise and fall, and high conductivity.

1.2 Plasma Generation Basics

This thesis involves the generation, manipulation, and diagnosis of plasmas in a laboratory setting. Plasmas are bodies of gas whose molecules have been excited to the point that a reasonable number of them ionize, or separate into ions and electrons. One can think of a plasma as the fourth state of matter beyond solid, liquid, and gas. In this research, the plasmas generated will be weakly ionized, meaning only a small fraction of the gas particles have been ionized, so mostly neutral particles are present. An ionized plasma is by definition a neutral body, meaning the number of free electrons is equal to the number of ions. The presence of free electrons and ions make it electrically conductive.

Plasma is the most abundant state of matter in the universe: stars are bodies of ionized gas. Fire, lightning, and the ionosphere are other naturally occurring plasmas. Fluorescent lighting is a common man-made plasma. Plasma is important in many areas of research,

and can be a dangerous phenomenon that must be accounted for or eliminated. Upon re-entry, the glow around a spacecraft is actually a plasma generated by the friction of the vessel in the atmosphere. Special heat-dissipating tiles are used on space shuttles to protect the airframe from the plasma's high temperature. High potentials in power distribution systems can generate plasma similar to lightning in explosive arc discharges. Equipment must be carefully installed to avoid this problem. Fusion reactors generate extremely hot plasmas that are difficult to contain. Strong magnetic fields are used to confine fusion-generated plasmas. A few examples of plasmas, along with their temperatures, are shown in Figure 1.2

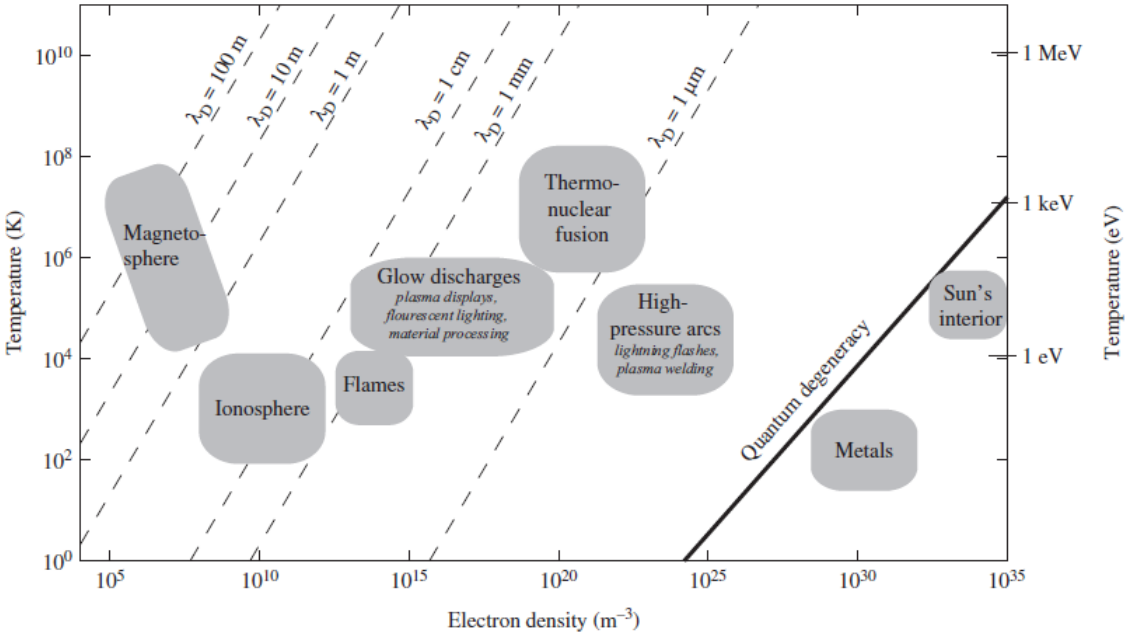

Figure 1.2: Types of plasma and their parameters from [3].

There are many possible means by which a plasma can be generated and maintained. In a laboratory setting, the most straightforward way is to generate an electric field high enough to create conventional breakdown. A gas at a given pressure can be assigned a dielectric strength. When the electrical field applied to a gas overcomes this dielectric strength, the molecules begin to ionize. The electric field in this research will be generated

between two electrodes. The law describing the minimum electric field between electrodes at which breakdown occurs is known as Paschen's law. The presumption is that the electric field is generated by two parallel-plate electrodes with a certain distance d, embedded in a gas with a certain pressure, which therefore has a minimum voltage that must be applied betwen the two plates in order to induce breakdown, first described in [4]. The Paschen curve is a graphical representation of Paschen's law, describing the breakdown threshold voltage as a function of pressure and electrode gap distance. The horizontal axis is in units of Torr-cm, so increasing the pressure by a factor of two is roughly equivalent to halving the separation between the plates. Example Paschen curves are shown in Figure 1.3, including the curve for Argon, which will be the gas used in this study. This idealized law presumes electrodes that are essentially infinite parallel plates, so for a different geometry, the curve will generally be different.

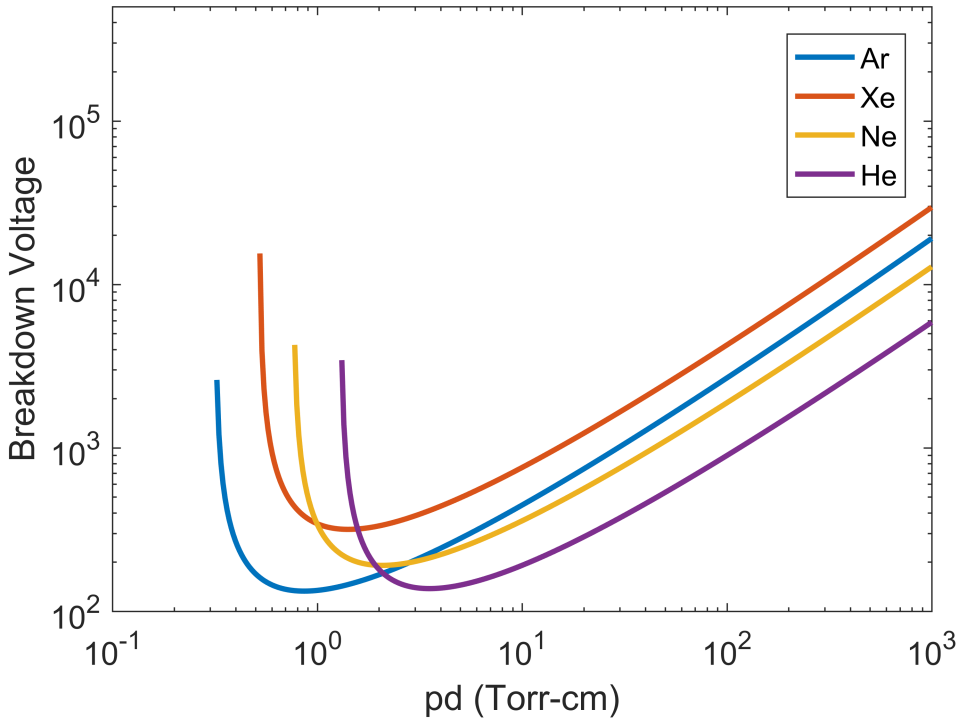

Figure 1.3: Paschen curves for a selection of gases using fit parameters from [5].

This curve varies with the type of gas used, and its fit parameters are determined em-

pirically. The range of test pressures in this study is limited due to the effects of Paschen's law and the ionizing voltage source's maximum output. A comparison of pulsed ionization data and the Paschen curve will be made in Section 3.2.3.

1.3 Plasma Antennas

The envisioned application for the work here relates to plasma antennas, but ours is not the first effort to consider a plasma as a conductor used for radio wave generation. Conventional antennas utilize metal as the conducting medium. At the simplest level, if the metal in a conventional antenna is replaced with a plasma column of the same size and shape, it in principle will exhibit the same radiation capability. An example of a basic plasma antenna used as an FM radio receiver is shown in [6]. A fluorescent bulb was used to generate the plasma, with a capacitive sleeve feed to couple the waves received in the antenna to the feed cable. This antenna is shown in Figure 1.4.

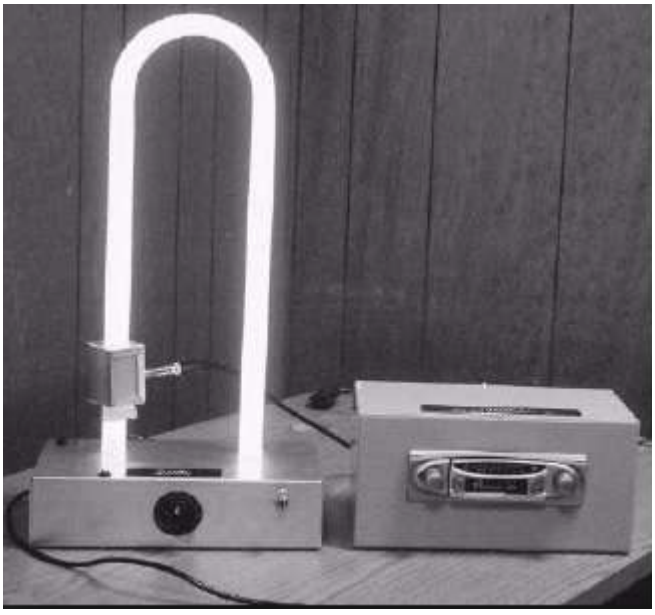

Figure 1.4: Fluorescent FM Plasma Antenna from [6].

The feed cable was connected to an FM radio tuner and a speaker. When fluorescent bulb was turned on, the gas inside is ionized. The FM signal was received by the antenna,

demodulated by the tuner, and music played through the speakers. When the bulb was turned off, the signal was no longer received, and only static played through the speakers. Plasma antennas have a few advantages over conventional antennas. They can be rapidly reconfigured, filter out high frequencies, and are electromagnetically invisible when de-ionized [7, 8]. Unfortunately, the complexity of plasma antennas render them impractical for many applications, namely that they require vacuum equipment, ionization circuitry, and glass tubes to contain the plasma.

1.4 Plasma Parameters

There is an incredibly rich history of laboratory experiments to demonstrate the electrical properties of plasmas, which we cannot adequately describe here, but we now proceed to give a basic description of plasma physics. To understand how a plasma reacts to an applied electric field, let us define its conductivity. It should be noted that we will be exclusively discussing plasmas that are isotropic, and do not have a significant static magnetic field affecting the electrical properties. This assumption cannot be made for most space plasmas [3]. Conductivity for a metal can typically be assumed to be a constant over a huge range of frequencies. For a plasma, however, that is not the case. This will be discussed in depth in Section 1.5. Let us first examine the key parameters that dominate plasma conductivity.

1.4.1 Electron Density

For a medium to conduct electricity, it must have free electrons present. The number of free electrons in a material per unit volume is referred to as electron density, N_e, measured in electrons/m^3. Copper, a common conductor, has an electron density of 8.49x10^{28}. Other metals have electron density values within the same order of magnitude. Glow discharge plasmas, such as those in fluorescent light bulbs used in basic plasma antennas, have an electron density on the order of 10^{14} [3]. It is beneficial for a plasma antenna's electron density to be as high as possible to support voltage propagation with low power dissipation.

Benchmarks for electron density will be set in Chapter 2.

1.4.2 Electron Temperature

The energy of a plasma's electrons is defined by their temperature, which is proportional to the average kinetic energy, or the square of the average velocity. Not all electrons are at the same kinetic energy. Electrons in a plasma travel at a wide range of velocities that, in many plasma studies, can be described by a Maxwellian distribution:

$$f(v) = 4\pi(\frac{m}{2\pi kT})^{\frac{3}{2}} v^2 e^{-\frac{mv^2}{2kT}}.$$

Where m is electron mass (often denoted m_e), m_e, and T is electron temperature (often denoted T_e). The shape of a Maxwellian distribution for electron velocity is set by electron temperature, with the average velocity $\langle v \rangle = \sqrt{\frac{8kT_e}{\pi m_e}}$. The average velocity is not the most probable velocity as the Maxwellian distribution is skewed positive. Examples of Maxwellian velocity distributions are shown in Figure 1.5.

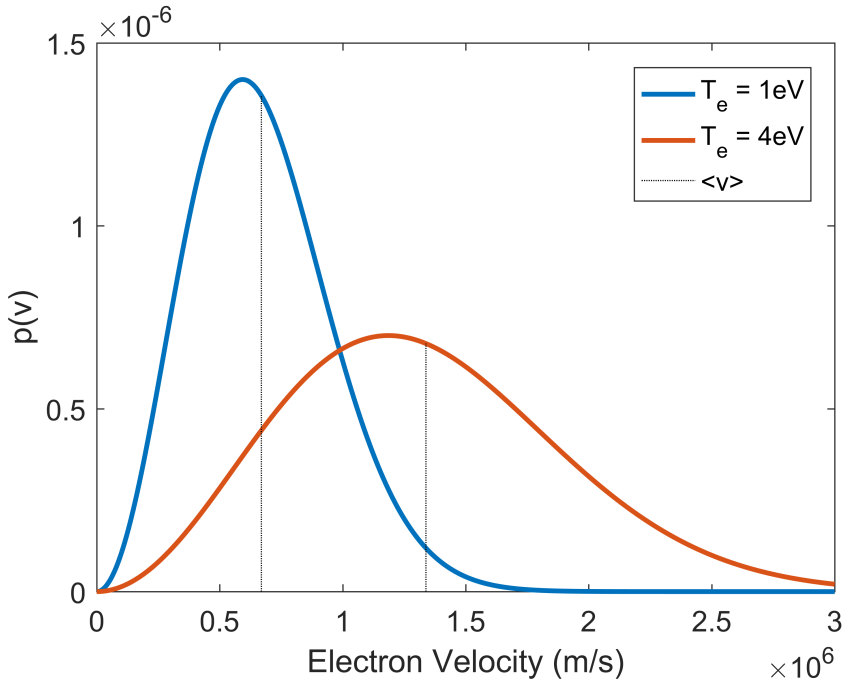

Figure 1.5: Electron velocity distribution of two electron temperatures. Note that 1 eV = 11,600 K.

Particle temperature can be measured in units of Kelvin, but for studies of charged particles such as those in plasma, the electronvolt is standard. One electronvolt is the energy an electron gains when accelerated through a potential difference of 1V, equivalent to 11,600 K [3]. The plasma generated in this research is a non-thermal, or cold plasma at low pressure. In this type of plasma, the electrons are at a much higher temperature than the ions and neutrals [9]. Even if the electrons are many thousands of Kelvin in temperature, you could still in principle put your hand in the plasma and not get burned. For this reason, non-thermal plasma is being explored as a possible method of sterilization. Low pressures mean less particles are present, so electrons are less likely to collide with neutrals and lose energy, resulting in higher temperature. While the overall temperature of the plasma may be near room temperature, the electron temperature can be expected to be much higher, on the order of 1 eV.

1.4.3 Collision Frequency

Collision frequency in a plasma, denoted ν, is the number of times per second a given species (neutrals, ions, or electrons) collides with another species. In fully ionized plasmas, collisions only occur between charged particles: ions to ions, electrons to electrons, or ions to electrons. The plasma generated in the lab experiments for the purposes of this research are weakly ionized, thus electron-neutral collisions are the dominant collision process, because there are many fewer charged particles than there are neutral particles. Although there are an equal number of ions and electrons, the ions are substantially heavier and thus have much lower velocity even at the same temperature, and thus collide very rarely compared to electrons. In weakly ionized plasmas, neutral particles impede electron motion, resulting in electrons losing some or all of their momentum during collisions [3]. The likelihood of one of these collisions is a factor of three things: gas density, the cross section of neutral particles, and the average velocity of electrons. Electron-neutral collision frequency is expressed as $\nu_{en} = N\sigma\langle v\rangle$, where N is gas number density, σ_{en} is the neutral particle cross section, and $\langle v\rangle$ is the average electron velocity. Gas number density N can be described as a pressure using a form of the ideal gas law: $N = \frac{P}{kT}$, where P pressure is in Pascals, T is ambient temperature, and k is the Boltzmann constant. In this research, we use Torr as pressure units, so a conversion factor of 133.322 Pa/Torr is included in the calculations. Next, electron cross-section σ is calculated using the radius r of the neutral particle, argon, which is 71 pm. Cross-section is simply calculated as $\sigma = \pi r^2$. Finally, average electron velocity is $\langle v\rangle = \sqrt{\frac{8kT_e}{\pi m_e}}$ as described in section 1.4.2. Another conversion factor of 11,600 K/eV is added here so the plasma temperature can be expressed in eV. Finally, all of these equations and conversion factors can be combined and simplified into a useful form:

$$\nu_{en} = \frac{40614r^2P}{T}\sqrt{\frac{\pi T_e}{km_e}}$$

where the experimetal inputs to this equation are vessel pressure P, ambient temperature T in Kelvin, and electron temperature T_e in electronvolts. For brevity, since only one type of collision dominates, the frequency will be expressed as ν, dropping the subscripts.

1.5 Plasma Conductivity

For an isotropic (unmagnetized) plasma, the AC conductivity is

$$\sigma = \frac{N_e q_e^2 (\nu - j\omega)}{m_e(\nu^2 + \omega^2)}$$

as shown in [3]. Conductivity in a plasma is dependent on a plasma's collision frequency and electron density, as well as wave frequency ω. The dependence on wave frequency means that a plasma column for use as an antenna must be carefully designed so that it will conduct at the operating frequencies of interest. In this case, the frequencies of interest are not VLF/LF, but much higher frequencies as we will discuss later. A common metric of a plasma's ability to conduct an electromagnetic frequency is plasma frequency:

$$\omega_p = \sqrt{\frac{N_e q_e^2}{\epsilon_0 m_e}}.$$

Plasma frequency is a measure of the degree of ionization in a plasma. When $\omega << \omega_p$, plasma a good conductor, while when $\omega >> \omega_p$, plasma is a poor conductor and is invisible to electromagnetic waves [6]. For a plasma antenna to behave like a good low-loss conductor, its operating frequencies must be well below the plasma frequency. This is apparent in Figure 1.6, where we have plotted the conductivity (vertical axis) against frequency (horizontal axis), for a plasma with electron density of 10^{18}. The hypothetical plasma in the figure has a plasma frequency of 56.4 GHz, shown with the vertical dashed black line. Its real conductivity is approximately constant until 1 MHz, when it starts rolling off. Its imaginary conductivity is approximately zero until it reaches a resonance null around 20 MHz. The peak in imaginary conductivity occurs in the middle of the

real conductivity's rolloff. The change in the imaginary component of conductivity can be interpreted as a change in its permittivity value ϵ. A change in permittivity causes a change in wave velocity as seen in the wave velocity equation: $v_p = \frac{1}{\sqrt{\mu_o \epsilon}}$. At the plasma frequency, the plasma is clearly non-conductive. To minimize loss and distortion, the operating frequency should be in the range where the real part of conductivity is flat, and the imaginary part of conductivity is approximately zero. For this particular example, the conductivity is fairly constant with frequency until 2 MHz. This is substantially less than the 56.4 GHz plasma frequency, and demonstrates that collisions effectively reduce the apparent plasma turnover frequency.

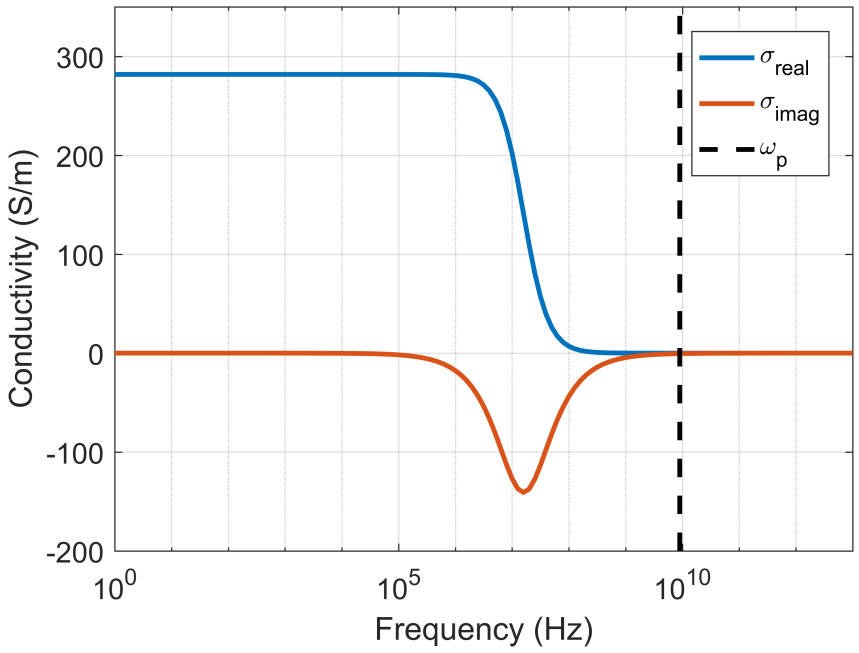

Figure 1.6: Real and imaginary components of conductivity for a theoretical plasma (N_e=10^{18} and ν=10^8) vs. frequency.

Compared to conventional metal conductors, this hypothetical plasma's conductivity is quite low. Its maximum real conductivity value is 281.7 S/m, while copper's conductivity is 5.96x10^7 S/m. For a 1 cm radius column of this plasma, resistivity is 11 Ω/m. Ohmic losses are negligible over a few meters with this resistivity.

1.6 Measuring Plasma Parameters

To determine a plasma's conductivity, its electron density and collision frequency must be measured. Collision frequency is difficult to measure directly, so it can be calculated from the plasma's electron temperature as discussed in Section 1.4.3. These parameters can be measured directly by inserting probes into the plasma, or through noninvasive optical emissions analysis.

1.6.1 Langmuir Probes

The easiest diagnostic tool to implement is the Langmuir probe. A Langmuir probe is a wire immersed in the test plasma. Various voltages are applied to the wire while current flow is measured. Plotting the measured current against the applied voltages yields a current-voltage, or I-V curve, which is analyzed to determine the plasma's parameters. An ideal example of an I-V curve is shown in Figure 1.7.

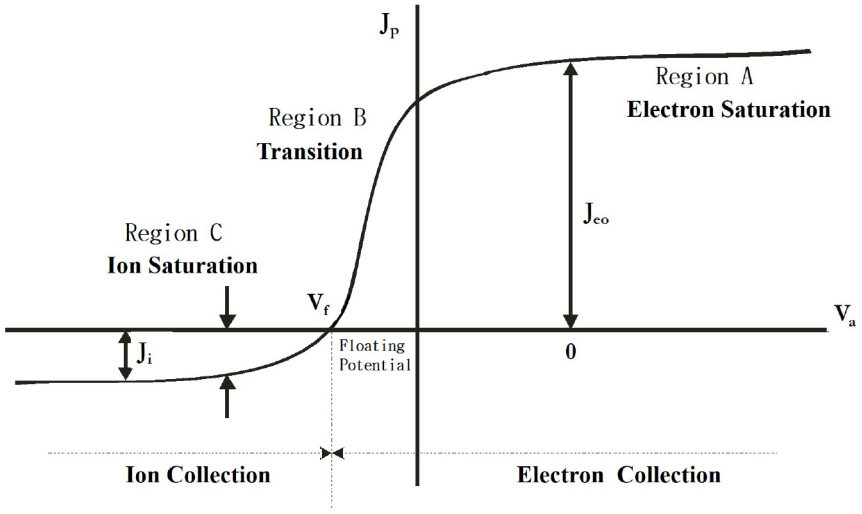

Figure 1.7: I-V Plot of a Langmuir probe, from [10].

The explanation of the regions of an I-V curve below comes from [11]. The current measured by the probe is the sum of ion current I_i and electron current I_e (J, current density, is used in lieu of I, current, in the figure). The floating potential V_f is the point at which

electron and ion currents are equal. At voltages below V_f, the probe is repelling electrons and collection ions. At voltages far below V_f where the all electrons have been repelled, the curve has reached I_{ist}: ion saturation. At voltages just above V_f, the curve enters the transition region in which electrons are only partially repelled by the probe's potential. If the plasma has a Maxwellian velocity distribution, the transition region is exponential. At even higher probe voltages the curve begins to flatten out, entering the electron saturation region, I_{est}. In this region, electron current increases slowly as voltage increases due to plasma sheath expansion. Hiden Analytical summarizes the Orbital Motion Limited (OML) Technique for Langmuir probe I-V curve analysis in [12]. To infer the density and temperature of the plasma's electrons, its electron current I_e must first be isolated from its ion current I_i. First, the section of the I-V curve in the ion saturation region is plotted as I^2 vs. V, and a line is fit to the modified data. The square root of this fit line is taken and subtracted from the original I-V curve, leaving only I_e. The natural logarithm of I_e is plotted against V as shown in Figure 1.8.

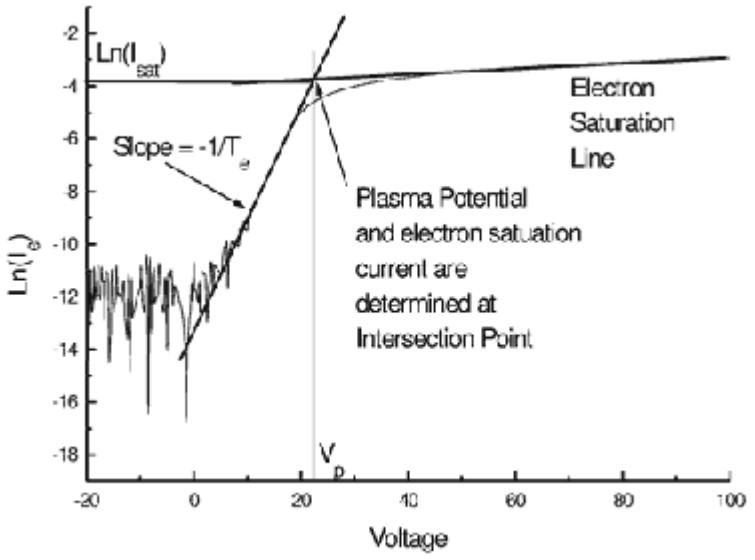

Figure 1.8: Natural logarithm of electron current, from [12].

The plasma parameters can be inferred from this plot. A line is fit to the section of the

plot corresponding to the transition region, which gives electron temperature in eV as

$$T_e = \frac{1}{Slope}.$$

Another line is fit to the electron saturation region. The intersection of the electron saturation fit line and the transition region fit line yields $ln(I_{est})$, which is easily converted to I_{est}. Finally, electron density is calculated as

$$N_e = 3.73x10^{13} \frac{I_{est}(amps)}{A_p(m^2)\sqrt{T_e(eV)}}$$

where A_p is probe surface area.

1.6.2 Optical Methods

When a plasma is excited, its atoms' electrons transition from ground state energy levels to higher order energy levels. De-ionization processes begin immediately as a plasma is ionized, resulting in electron transitions from higher energy levels to lower or ground state energy levels. These transitions cause photon emission at a species-specific set of wavelengths following the equation

$$\lambda = \frac{hc}{E_h - E_l}$$

where E_h and E_l are the higher and lower order energy levels. A given atom has a unique set of emission wavelengths based on its energy levels. The intensity of light at each wavelength is primarily a function of the plasma's electron temperature and gas pressure [13]. As a plasma becomes more energetic, higher energy photons are emitted, and line intensities vary. Optical emission spectroscopy (OES) is used to measure a plasma's line intensities over a range of wavelengths. The line ratio method is commonly used to analyze OES data by comparing measured line intensities to calculated intensities via a Collisional Ra-

diative model (CRM) [14]. The CRM used in this research is PrismSPECT, which will be discussed in Chapter 4.

CHAPTER 2
VOLTAGE PULSE ATTENUATION IN PLASMA

At a high level, we need to establish what kind of plasma properties will enable the reflection suppression antenna described in Chapter 1 to work efficiently. One key benchmark is the conductivity, which must be high enough to support voltage pulse propagation across the plasma column. In this chapter, we will quantify this benchmark by simulating the plasma properties and wave attenuation. In any real antenna, the conductor will be imperfect, leading to some resistive losses. The frequency-varying resistance of plasmas result in higher than normal loss when compared to metal antennas at high frequencies. Our goal in this chapter is to set the requirements for a plasma to have high enough conductivity that it conducts the voltage pulses with little to no attenuation. To quantify the plasma requirements, we will now describe a model of voltage attenuation along a plasma column as a function of key plasma parameters. We will assume that the pulses fed into the antenna are approximately Gaussian. A Gaussian pulse has a wide band of frequency content. For example, a Gaussian pulse with 1 ns standard deviation has frequency content that extends in the 100s of MHz to GHz range. Because a plasma is not a good conductor above the plasma frequency, pulses with frequency content above the plasma frequency will be attenuated and distorted. As such, our goal of conducting short pulses requires a fairly high plasma frequency, and therefore a high electron density. We will utilize transmission line theory to determine how well a given plasma column will conduct a pulse with a certain duration.

2.1 Transmission Line Wave Propagation

Our approach is to consider the plasma channel as a transmission line, which is a conductor that is capable of propagating both voltage and current from one end to another, with a

nonzero and quantifiable delay. A transmission line can be thought of as a chained series of inductors and capacitors, each of which impede and slow down the transmission of voltage and current as shown in Figure 2.1.

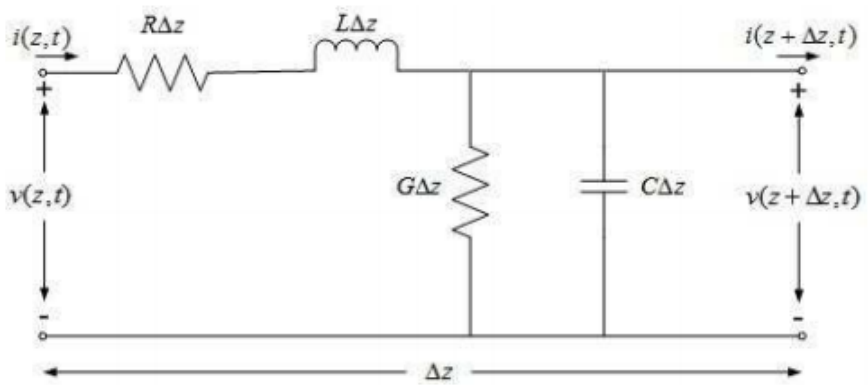

Figure 2.1: Transmission line as circuit components [15].

The Telegrapher's equations uses the circuit component model to predict voltage and current wave propagation down a transmission line as functions of line parameters, spatial position, and time:

$$\frac{\partial z V(z,t)}{\partial z} = -(R + L\frac{\partial}{\partial t})I(z,t)$$

$$\frac{\partial z I(z,t)}{\partial z} = -(G + C\frac{\partial}{\partial t})V(z,t).$$

The equation for a waves traveling on a transmission line is derived from the Telegrapher's equations as

$$V(z) = V^{+}e^{-\gamma z} + V^{-}e^{\gamma z}$$

where V^{+} is the initial magnitude of a forward traveling wave, V^{-} is that of a backward traveling wave, and z is position in meters. We consider only the forward traveling wave here. The propagation constant γ combines transmission line parameters as

$$\gamma = \sqrt{(j\omega L + R)(j\omega C + G)}$$

where L is inductance (H/m), C is capacitance (F/m), G is conductance (S/m), and R is resistance (Ω/m) [16]. For a lossless transmission line, conductance and resistance by definition are set to zero. However, a plasma column is modeled as a lossy transmission line due to its low conductivity. Conventional lossy transmission lines are run in the time domain since the resistance R is constant with frequency. However, in our case, the plasma resistance is frequency-dependent. Thus, we will have to apply this model in the frequency domain. Conductance is set to zero in our model, as ohmic losses will be the dominant source of attenuation. The propagation constant can be separated into real and imaginary terms as $\gamma = \alpha + j\beta$. α is an exponential decay constant, describing voltage wave attenuation due to resistive loss. The imaginary part of the propagation constant β describes the wave propagation properties such as phase and group velocity. The velocity of a wave on a transmission line is controlled by line inductance (H/m) and capacitance (F/m), following the relationship

$$v_p = \frac{1}{\sqrt{LC}},$$

measured in meters per second. The focus of this study is on the effects of line resistance, so the inductance and capacitance are chosen so that v_p is equal to vacuum speed of light propagation.

2.2 Plasma Resistance Function

Once the conductivity is known, the resistance of a plasma is found from equation

$$R = \frac{1}{\sigma A}$$

with units of Ω/m, where A is the cross sectional area of the plasma column in m^2. A large cross section reduces resistance, therefore the diameter of the plasma column should be as high as possible. Because plasma conductivity is in general a complex number, its resistance is complex as well. The imaginary component of the resistance contributes to β

in the wave equation, which affects the propagation velocity. The real component of resistance contributes to the attenuation constant. Here, the real component of resistance is our primary focus due to its contributions to ohmic loss. Similar to the conductivity plot from Chapter 1, resistance vs. frequency is plotted in Figure 2.2 for plasma parameters $N_e=10^{18}$ and $\nu=10^8$. As the wave frequency nears the plasma frequency, resistance increases sharply.

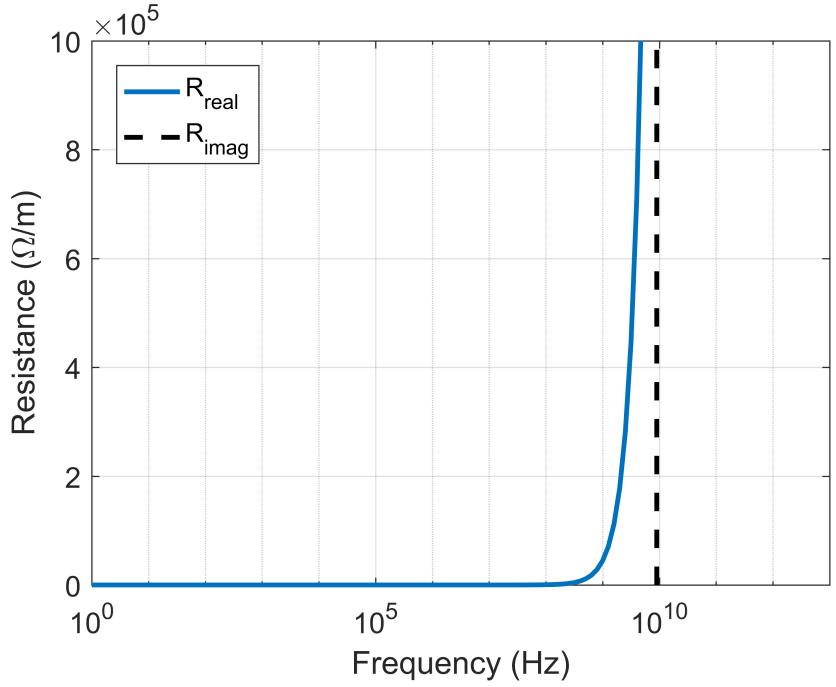

Figure 2.2: Resistance of a theoretical plasma ($N_e=10^{18}$ and $\nu=10^8$) vs frequency.

2.3 Pulse Frequency Content

To model how a pulse is attenuated and distorted in a plasma, its spectral content is found via Fourier transform methods. Through Fourier analysis, any time-domain signal can be treated as a sum of sinusoidal signals at many different frequencies, with a combination of amplitudes and phases. The Fast Fourier Transform is a simple numerical method to implement that yields the magnitude and phase of the frequency components of a signal. A Gaussian signal's spectral content depends on its length in time. The equation for a

Gaussian pulse centered around zero is

$$v(t) = e^{\frac{t^2}{2\sigma^2}}$$

where σ is the standard deviation, which sets the width of the curve. Throughout the thesis, we define pulse duration as the length of time an input pulse's voltage is greater than zero, with the Gaussian standard deviation set equal to one-eighth of the pulse's duration. Examples of Gaussian pulses 1 nanosecond and 5 nanoseconds wide and their frequency content are shown in Figure 2.3.

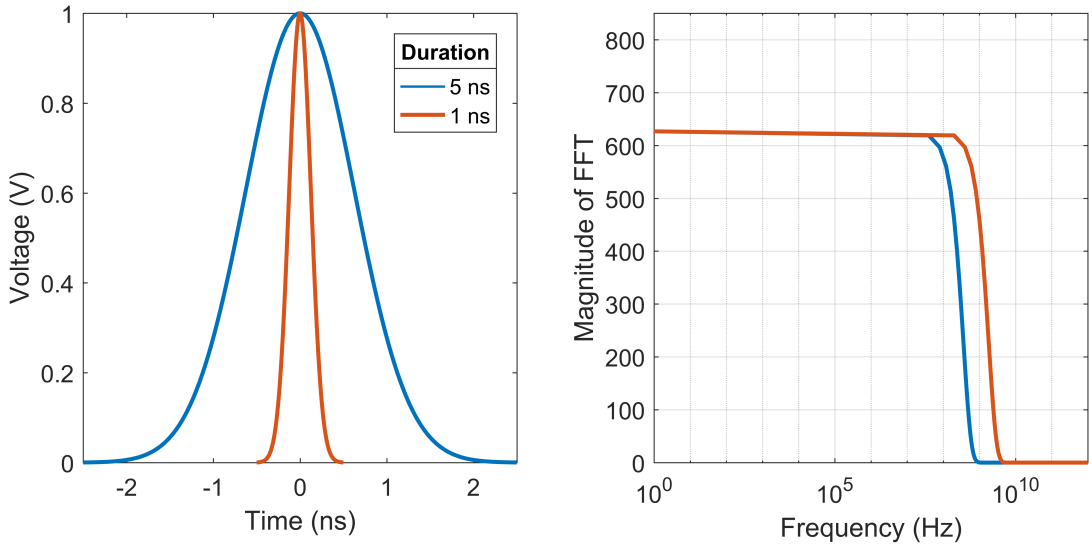

Figure 2.3: Gaussian pulses at multiple widths (left) and their frequency content (right).

The resistance function for the theoretical plasma is shown in Figure 2.2 and resembles a lowpass filter, but the turnover frequency increases as pulse duration is reduced.

2.4 Pulse Attenuation Modeling

We can now describe our pulse propagation mode in detail. The wave propagation equation is applied at each frequency component of the pulse to determine how much power is dissipated as it travels through the antenna. First, the frequency components of the pulse are

calculated by the FFT. The plasma's parameters (electron density and collision frequency) are then used to calculate the plasma resistance as a function of frequency, which is used to find the propagation constant γ for each frequency. The propagation constants are used in the equation for a forward traveling wave to determine the degree of attenuation of each frequency component when the pulse reaches the end of the antenna. The attenuation function is applied to the original pulse's spectral content. The inverse FFT is applied to the pulse's attenuated spectral content, ultimately yielding the pulse's shape at the end of the antenna. The pulses can be assigned a physical width according to their duration and the propagation velocity. For the reflection suppression concept to be realized, a pulse must be able to fit entirely in one of the antenna's sections. A 1 nanosecond long pulse traveling at the speed of light is 30 centimeters long in space. The physical length of the pulses imposes a minimum length restriction on the plasma cells. To increase antenna efficiency, multiple voltage pulses need to be traveling down the antenna concurrently, so short plasma cells are desirable, once again relying on the plasma's conductivity. The plots below show the output of the pulse propagation code for a variety of pulse widths and theoretical plasmas.

2.4.1 Model Run Examples

A collision frequency on the order of 1 GHz is calculated for the range of test pressures and electron temperatures. The antenna length is set to 3 meters long with a radius of 2 centimeters. Pulse lengths of 1 ns and 5 ns propagating through plasma modeled below. The vertical axis is voltage, while the horizontal axis is time. The blue curve is the Gaussian pulse at the antenna feed before propagation. The red curve is the pulse after it has traveled three meters down a plasma column with N_e=10^{19} /m^3 and ν=10^8 /s. As expected, the 1 ns long pulse is attenuated more than the 5 ns long pulse. The higher frequency content in the shorter 1 GHz pulse is above the plasma frequency, causing more lossy propagation.

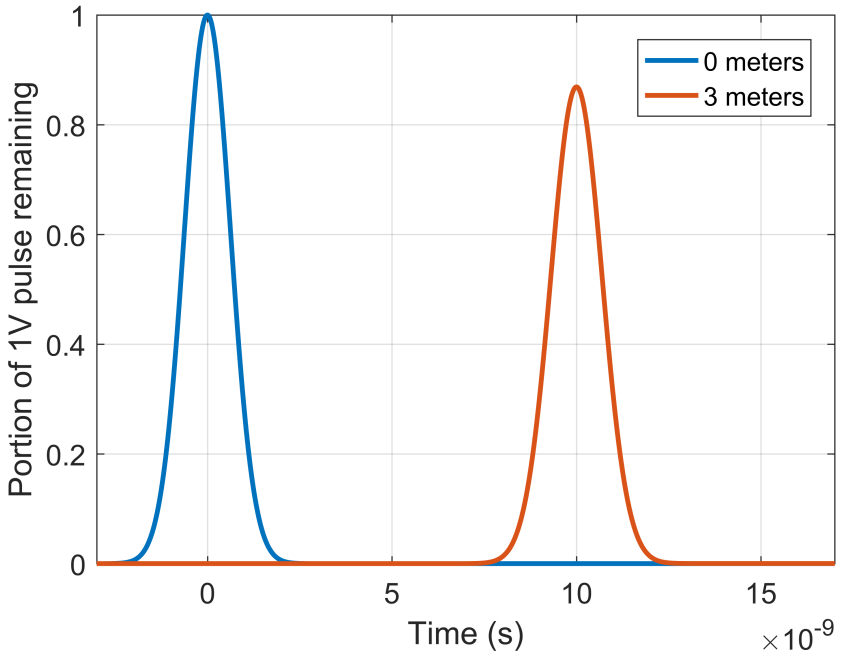

Figure 2.4: Attenuation of 5 ns pulse in a plasma column with theoretical parameters.

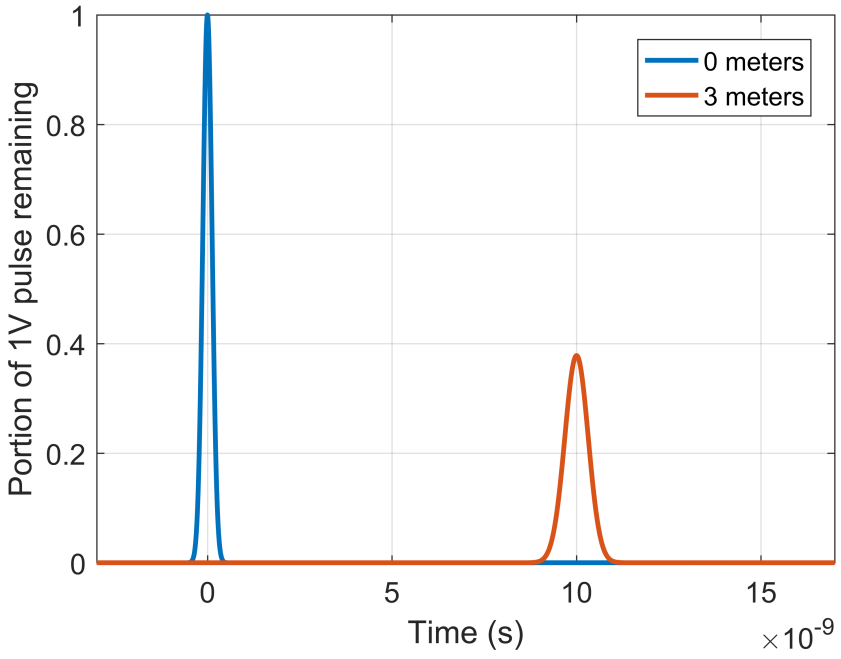

Figure 2.5: Attenuation of 1 ns pulse in a plasma column with theoretical parameters.

2.4.2 Model Applications

Having now established a model for a voltage pulse's behavior as it propagates down a plasma channel with certain properties, the next step in subsequent chapters is to determine actual measured plasma parameters. We will then feed these more realistic measured values into this model to determine the shortest pulse the plasma can conduct with minimal attenuation.

CHAPTER 3

MEASUREMENTS

To apply the pulse attenuation model to real data, a plasma column must be generated and analyzed. In this chapter, we discuss the details of the plasma generation equipment, measurement instrumentation, and measured results. The first type of measurements discussed are taken with a photodetector. These are used to determine the plasma's speed as test pressure and voltage are varied. The plasma's ionization and de-ionization speed are important for the pulse-blocking matching technique. Next, Langmuir probe measurements are used to analyze the plasma's electron temperature and density. Finally, spectrometer measurements are used to record the plasma's emissions. Langmuir probe measurements and spectrometer measurements both yield electron temperature and density.

3.1 Experimental Setup

3.1.1 Plasma Generation Equipment

The details of the plasma chamber's design and previous versions are detailed in [17]. The chamber consists of a Pyrex glass tube between two 4.5 inch ConFlat (CF) crosses. The plasma generating electrodes are placed in the tube for testing. One end of the chamber is used for vacuum pumping, and the other for gas flow. An Adixen 2121SD roughing pump on the vacuum control end of the chamber is used to evacuate the system to around 10 mTorr. Chamber pressure is monitored by a KJLC 375 gauge controller and KJLC 257 Pirani tube. Once the chamber has been evacuated, the plasma's background gas is introduced to the system. Gas flows from a tank of ultra-high purity argon through an Airgas Y11-215D pressure regulator to a custom flow control manifold. The manifold uses an MKS 1179A mass flow regulator and an MKS 247D control unit to guarantee a

consistent flow rate into the chamber. These control units are set to provide their maximum gas flow rate. Pressure is controlled manually on the vacuum control end of the chamber. A bellows valve used to isolate the vacuum pump from the chamber is used to restrict vacuum until the gauge reaches the desired test pressure.

Two different power supplies are used to ionize the plasma. The Lambda (GEN600-2.6) DC power supply is used to generate steady state DC plasma. This unit can supply up to 600 V and 2.6 A. The FID (FPG 1-50NM100A) high voltage pulse generator is used to generate nanosecond pulsed plasma. This unit can supply pulses from 500 to 1000 V with FWHM widths from 5 to 100 ns and up to 50 kHz repetition frequency. The pulses from this unit are designed to approximate square waveforms, but at these speeds the rise and fall of the pulses are noticeable. Figure 3.1 shows a 1 kV, 10 nanosecond long pulse trace from the unit's manual.

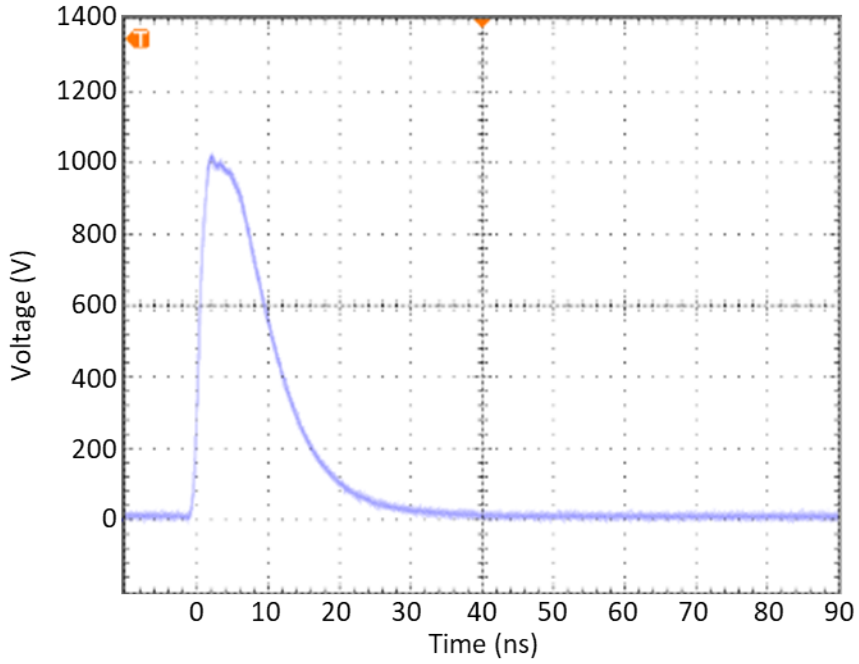

Figure 3.1: 1 kV, 10 ns pulse from FID pulser manual.

Electrode shape and spacing affects a plasma's behavior. Rectangular anodized aluminum electrodes (2.54 x 3.81 cm) were used for the light curve style measurements.

These were initially mounted with a 1.778 cm gap on custom fabricated epoxy laminate (G10) mounts. The gap length was reduced to 0.5 cm for later tests on custom ceramic (MACOR) mounts. The most recent electrodes are fashioned from aluminum round-top rivets set in MACOR mounts with a 1 cm gap. This mount is designed to hold a Langmuir probe in the body of the plasma for analysis. The rectangular electrodes in the 0.5 cm gap configuration are shown in Figure 3.2, and the rivet electrodes are shown in Figure 3.3.

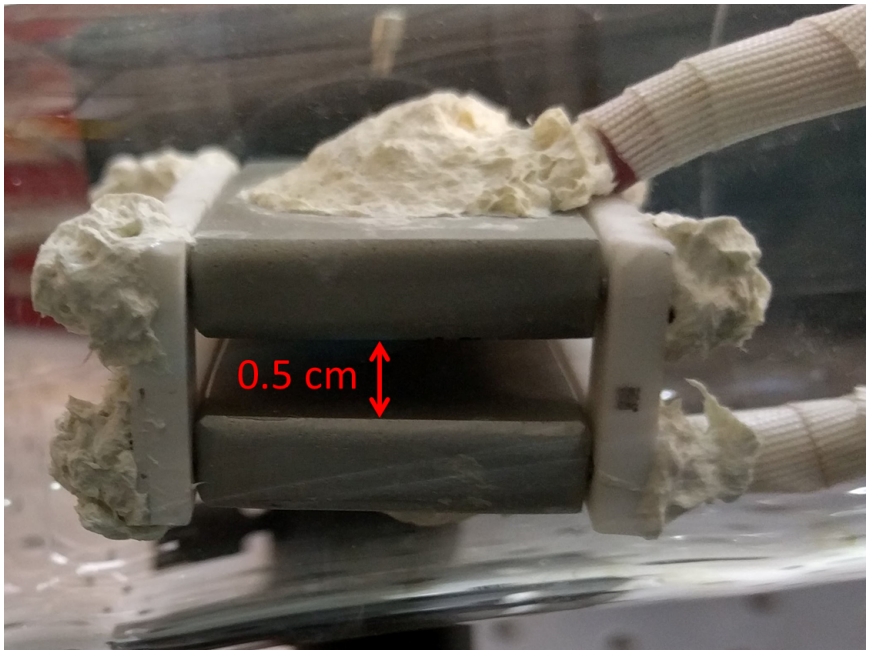

Figure 3.2: Rectangular electrodes at 0.5 cm gap length.

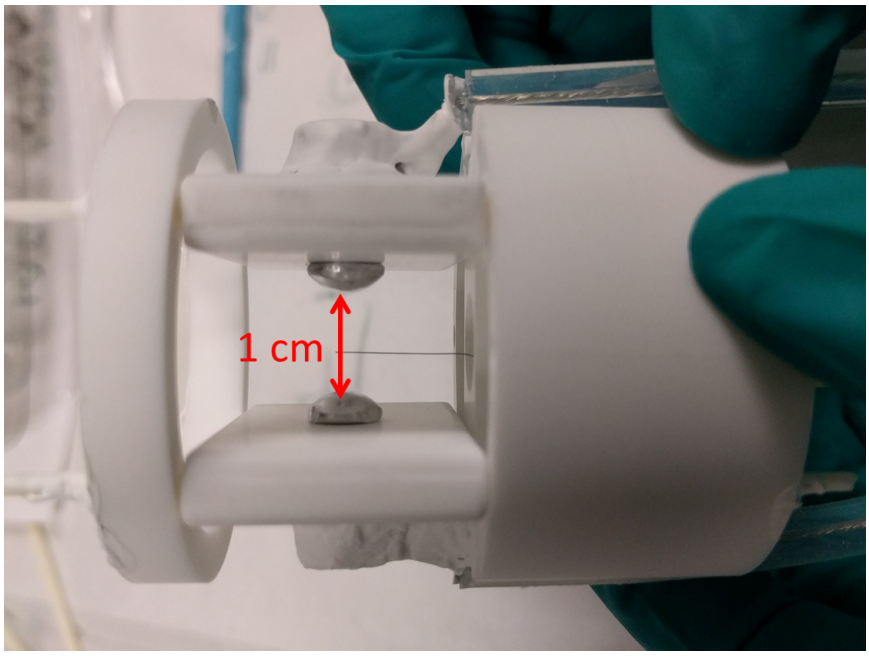

Figure 3.3: Rivet electrodes at 1 cm gap length. The wire between the electrodes is a Langmuir probe tip.

3.1.2 Plasma Analysis Instrumentation

Photodetector and spectrometer measurements are used to analyze the light emitted from the plasma. A Thorlabs APD430A2 variable-gain avalanche photodetector is used to record the plasma's total optical output as the plasma is modulated. This unit detects photons with wavelengths 200-1000 nm, outputting a voltage corresponding to the intensity of light detected. The photodetector is connected to a Tektronix DPO5104B oscilloscope to record voltage traces as a function of time. These traces, henceforth referred to as 'light curves,' are recorded via a LabView program provided by Tektronix. An Ocean Optics HR4000CF-UV-NIR asymmetric crossed Czerny-Tuner spectrometer is used to collect spectra data. This spectrometer has a wavelength range from 200 to 1100 nm. Each day the spectrometer is used, its wavelength and intensity axes are calibrated through the methods described in [17]. Intensity axis calibration can be a relative or absolute calibration. Absolute calibration provides a conversion between the analog-to-digital units used in a spectrometer to a power

density, while a relative calibration accounts only for the spectral sensitivity [13]. An absolute calibration provides more information about the plasma's spectra, but is difficult to perform. A relative calibration is sufficient for the line ratio method.

The Langmuir probes are built in-house from tungsten wire and ceramic tubing following specifications in [11]. A Keithley 2410 source meter is connected to the Langmuir probe to supply its bias voltage and measure the probe current. The source meter is controlled via LabView to sweep through the range of desired bias voltages and quickly generate I-V curves.

3.2 Photodetector Measurements

For the measurements in this section, the plasma is excited with the pulsed DC voltage source, operating at 5 nanosecond pulse width and 10 kHz pulse repetition frequency. The avalanche photodiode was used to record the plasma's optical emissions as it ionized and de-ionized, and to determine whether the plasma was extinguished between pulses.

3.2.1 Light Curves

To generate light curves, the plasma was monitored with the avalanche photodiode to track its optical output over time. The photodiode was connected to the oscilloscope to generate a voltage trace corresponding to optical emissions. Noise is introduced to the measurements by the pulser, apparent in Figure 3.4. The vertical axis is the photodectector output voltage, while the horizontal axis is time. Three parts of these light curves yield information about the rapidly ionized plasma: peak optical output, rise time, and fall time. When optical output is at its maximum, the plasma's ionization is strongest, therefore its electron density will be maximized. Rise and fall times for a curve are typically measured as the time it takes a curve to go from 10% of its maximum amplitude to 90% of its maximum amplitude. Here, we define rise time as the time it takes the light curve to go from 10% of its maximum amplitude to its maximum amplitude, and fall time from the maximum amplitude to 10%

of maximum. This change in definition is appropriate in this instance because we are interested in how long it takes the plasma to reach its maximum electron density when a pulse is applied. Smoothing must be applied to the decreasing section of the curves for fall time analysis. Noise spikes in the measurements made fall time calculations difficult to automate, so smoothing was applied to the falling edge of the curve. The processed version of the curve is shown in Figure 3.4, with annotations to show timing points.

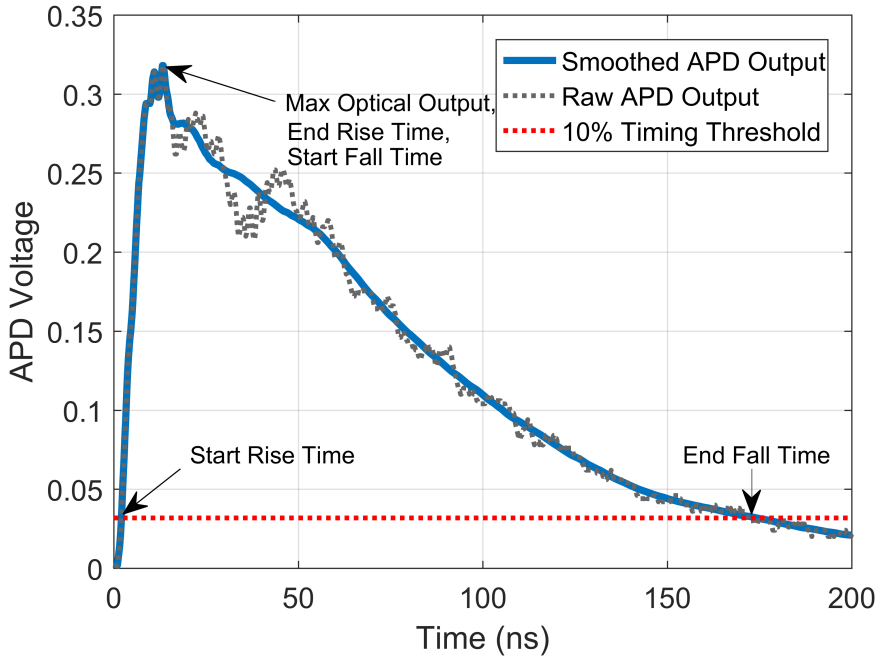

Figure 3.4: Raw and processed light curve from photodiode; response to 5 ns, 700 V pulse.

Ionizing voltage amplitude and background gas pressure affect a plasma's speed and electron density. To observe the effects of these variations, multiple light curves were taken at various pressures and ionizing voltages. In the plots below, the electrode gap size was 1.78 cm. Figure 3.5 shows the effects of varying voltage. As expected, higher ionizing voltages yield higher optical output, similar to increasing the voltage applied to a light bulb. Figure 3.6 shows the effects of varying background gas pressure. Varying pressure changes both the fall and rise times as well as the maximum optical output. Higher pressures at this gap size resulted in double peaks not seen at lower pressures. The double peaks were not

present at the other gap size tested, 0.5 cm.

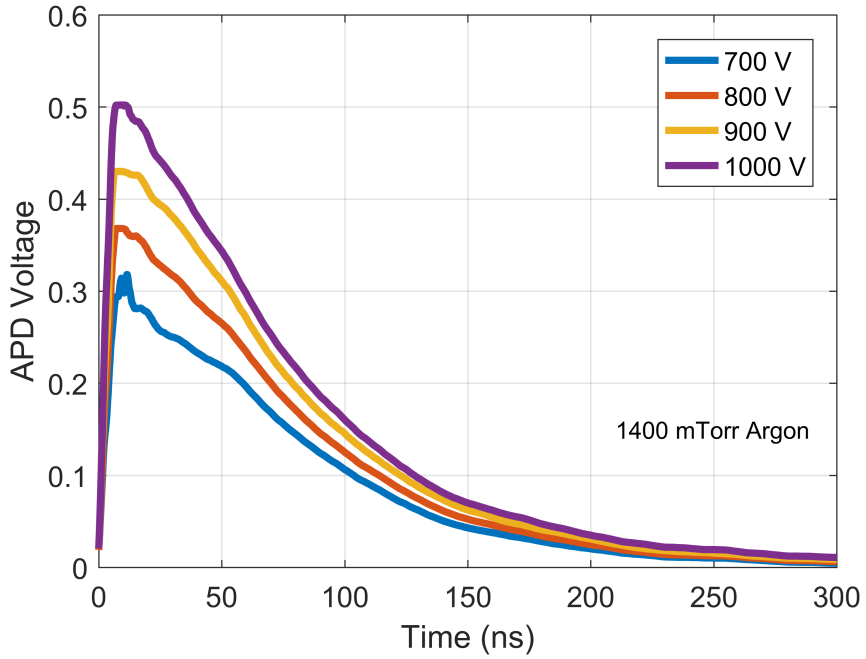

Figure 3.5: Light curves with fixed pressure, varying 5 ns ionizing voltage pulse amplitude.

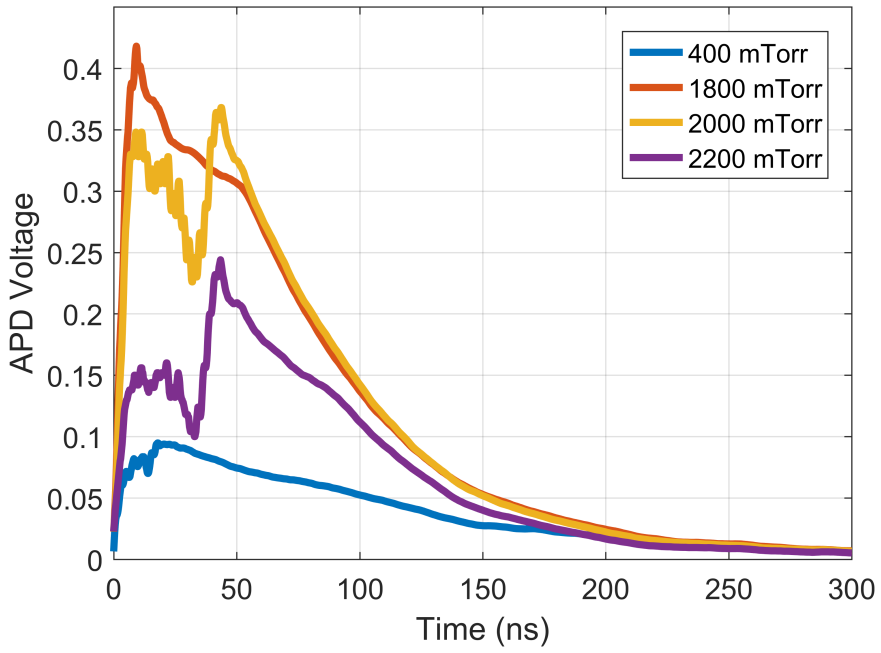

Figure 3.6: Light curves with 5 ns, 800V ionizing voltage, varying pressure.

3.2.2 Pressure-Voltage Sweeps

A pressure-voltage sweep is created by recording light curves at a range of pressures and ionizing voltages. Maximum photodetector output voltage, rise time, and fall time are extracted from the light curves. In this analysis, rise and time are defined as the time periods during which the photodetector output is between 10% of its maximum value and the maximum. For the sweep figures shown below, the ionizing pulse width was 5 nanoseconds long. This sweep analysis was performed at two different electrode gap lengths: 1.78 cm and 0.5 cm. Testing at the shorter gap length creates a stronger electric field, thus enabling higher-pressure plasma generation.

Figure 3.7 displays the maximum photodiode output sweeps. As expected, peak optical output always increases when ionization pulse amplitude increases. As pressure varies, the peak optical output has different trends at the two different gap lengths. At 1.78 cm, peak photodetector output is highest between 1500 and 2000 mTorr. At 0.5 cm, peak photodetector output increases as pressure increases and there is no ideal pressure range.

Figure 3.8 displays the rise time sweeps. Like the peak output sweep, the 1.78 cm gap rise times have a low rise time range. Higher pressures generally yield lower rise times, but at past 2000 mTorr rise time increased. The increase in rise time was caused by the double peak effect shown in the light curve plots. The double peak was only present in the 1.78 cm gap tests. The 0.5 cm gap rise times are generally lower as pressure is increased. An interesting anomaly occurs at 800 mTorr for the 0.5 cm gap tests, seemingly a rise time sweet spot at lower pressures.

Figure 3.9 displays the fall time sweeps. In both of these cases, the plasma fall time decreased with increasing pressure. This behavior is expected due to the linear relationship between pressure and collision frequency.

Figure 3.10 display the optical emission time. The time values here are dominated by fall time, which is around ten times higher than rise time in most cases. For the reflection suppression antenna to be efficient, combined ionization and de-ionization time needs to

be 10 nanoseconds or shorter. The shortest total emission time measured was 136 nanoseconds, much higher than the 10 nanosecond benchmark. However, the plasma's total optical output intensity does not yield information about the plasma's conductivity. As the plasma is ionized and de-ionized, its electron density varies. It is likely that the plasma does not need to be fully de-ionized to suppress a voltage pulse. The spectroscopic methods detailed in sections 4.2.1 and 4.2.2 will be used to determine the plasma's conductivity function as it is ionized and de-ionized.

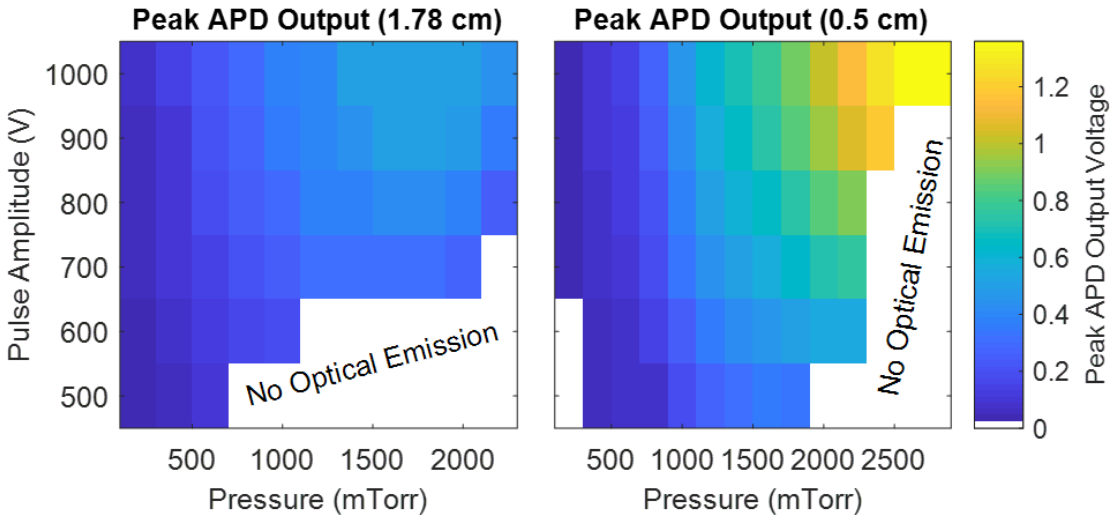

Figure 3.7: Peak optical output sweep with 5 ns ionization pulse at 1.78 cm and 0.5 cm gap lengths.

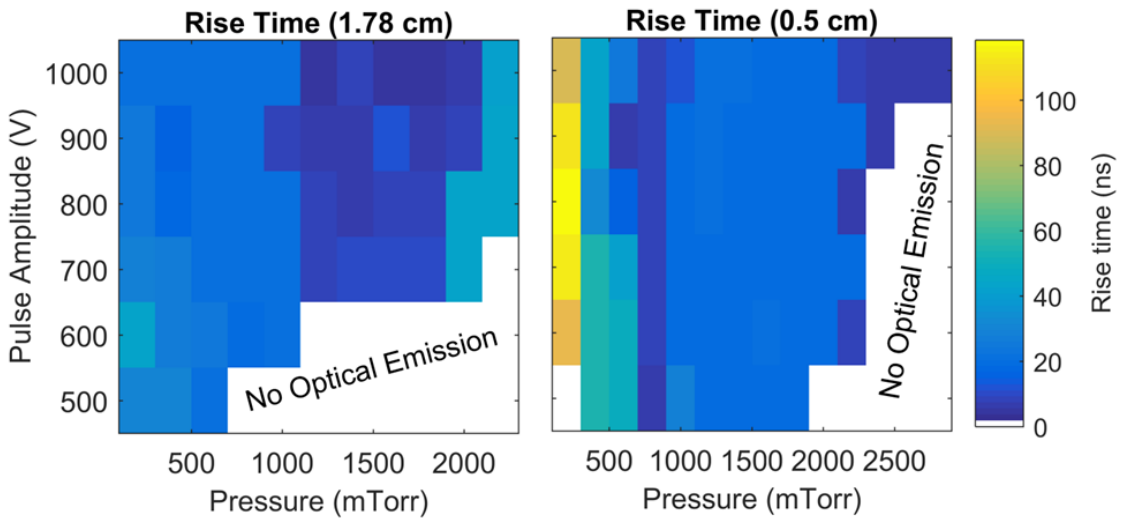

Figure 3.8: Rise time sweep with 5 ns ionization pulse at 1.78 cm and 0.5 cm gap lengths

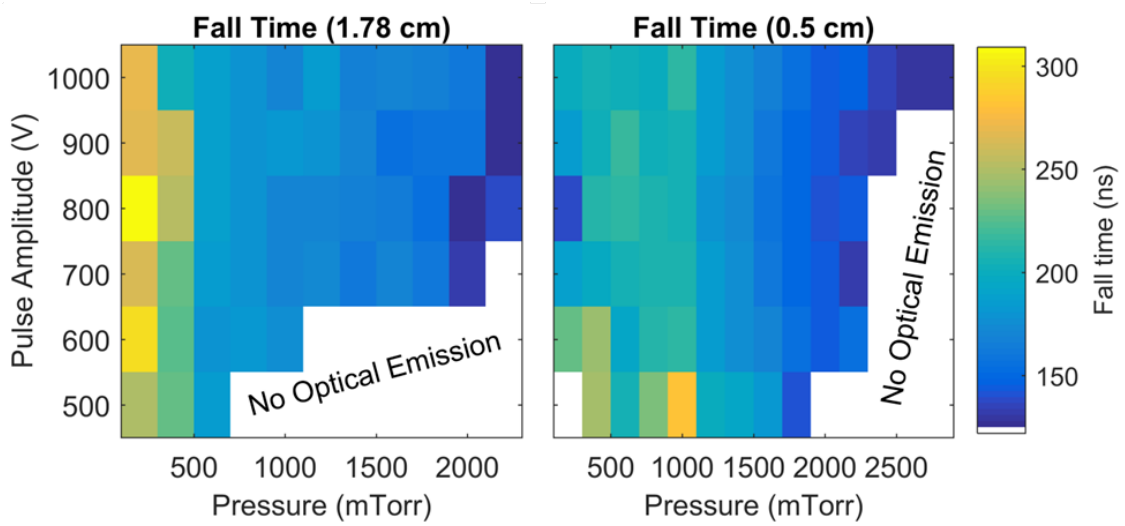

Figure 3.9: Fall time sweep with 5 ns ionization pulse at 1.78 cm and 0.5 cm gap lengths.

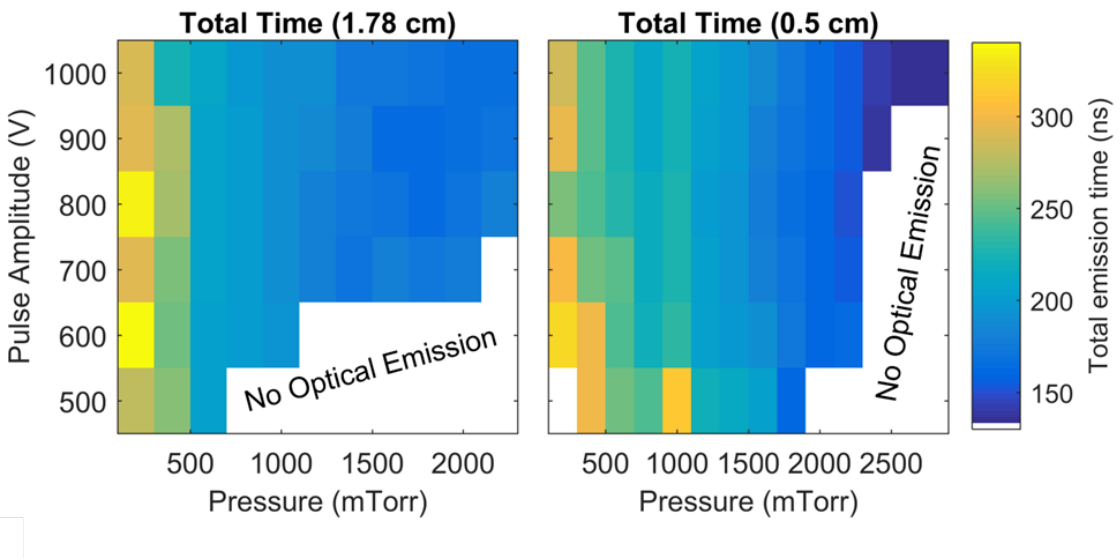

Figure 3.10: Total emission time sweep with 5 ns ionization pulse at 1.78 cm and 0.5 cm gap lengths.

3.2.3 Paschen Curve Comparison

By multiplying the electrode gap distance by each test pressure, the pressure-voltage sweep plots can be compared to the Paschen curve can be made as shown in Figure 3.11. The equation for the Paschen curve is $V_B = \frac{Bpd}{ln(Apd) - ln[ln(1+\frac{1}{\gamma_{SE}})]}$, where V_B is the breakdown voltage. A and B are gas-specific fit parameters. γ_{SE} is the second Townsend coefficient, which is dependent on electrode material [18]. The Townsend coefficient is often unknown and can be combined with the A fit parameter, becoming A', reducing the Paschen curve equation to $V_B = \frac{Bpd}{ln(A'pd)}$. A' and B are determined experimentally. Published values of A' vary between 2.64 and 3.57 cm-Torr, and B between 133 and 320 V/cm-Torr for argon [5]. For the 1.78 cm gap, A' = 3.1 cm-Torr and B = 320 V/cm-Torr provided the best fit. For the 0.5 cm gap, A' = 3.57 cm-Torr and B = 320 V/cm-Torr provided the best fit.

The experimental threshold voltages fell above the Paschen curve at most pressures. For the 0.5 cm gap tests, ionization was observed below the Paschen curve threshold for some of the lower pressures. Typical Paschen curve experiments are performed with DC

ionizing voltages and low-capacitance pin electrodes. Here, nanosecond pulses powered high-capacitance square electrodes. The differences in experimental design result in significant deviations from the typical Paschen curve. Here, nanosecond pulses powered higher capacitance square electrodes. Oscilloscope readings of the ionization feed show the voltage pulses reflecting back and forth in the cable. Thus, the full potential of each pulse is not utilized in the ionization process. This phenomena is seen in transmission line theory with transient pulses. The voltage feed lines are terminated in a complex impedance load, with both the capacitance from the square electrode design and the resistance from the anodized layer on the electrodes contributing to the reflections. Performing this test with DC ionizing voltage should result in a Paschen curve fit coefficients similar to those seen in other experiments, allowing steady-state conditions to be met. The sub-Paschen curve ionization may be due to an inaccurate pressure gauge.

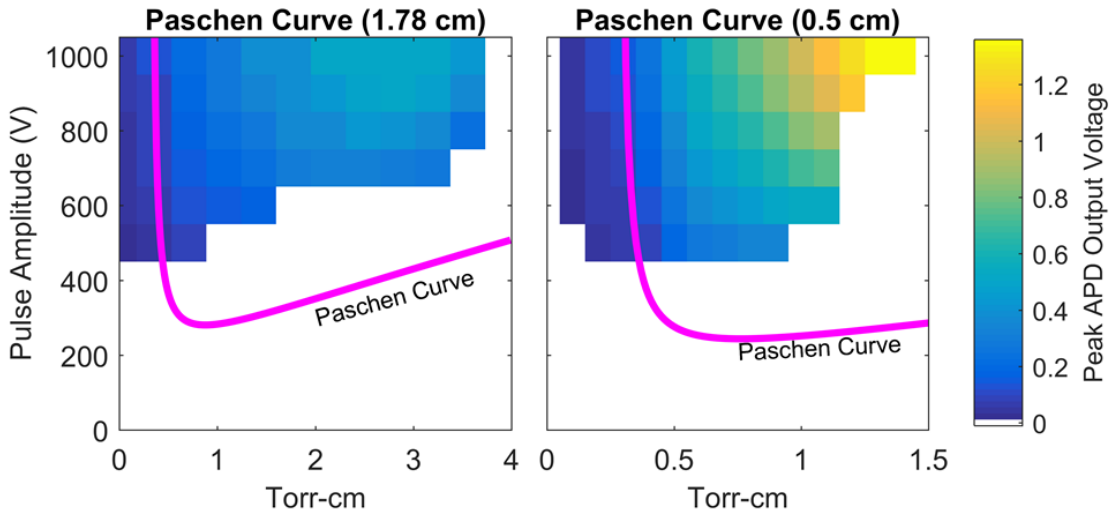

Figure 3.11: Paschen curve overlay at 1.78 cm and 0.5 cm gap lengths.

3.3 DC Plasma Measurements

3.3.1 Langmuir Probe

The DC Langmuir probe measurements were meant to serve as a baseline comparison for the PrismSpect line ratio methods. Unfortunately, the electrodes and power supply were unable to support a plasma column with enough volume to fully immerse the Langmuir probe tip. Ionization was induced with the DC power supply around 300 volts. The voltage could be increased to around 450 V before the plasma became unstable. Past 450 V, the electrodes arced uncontrollably. Figure 3.12 shows the plasma during a Langmuir probe test.

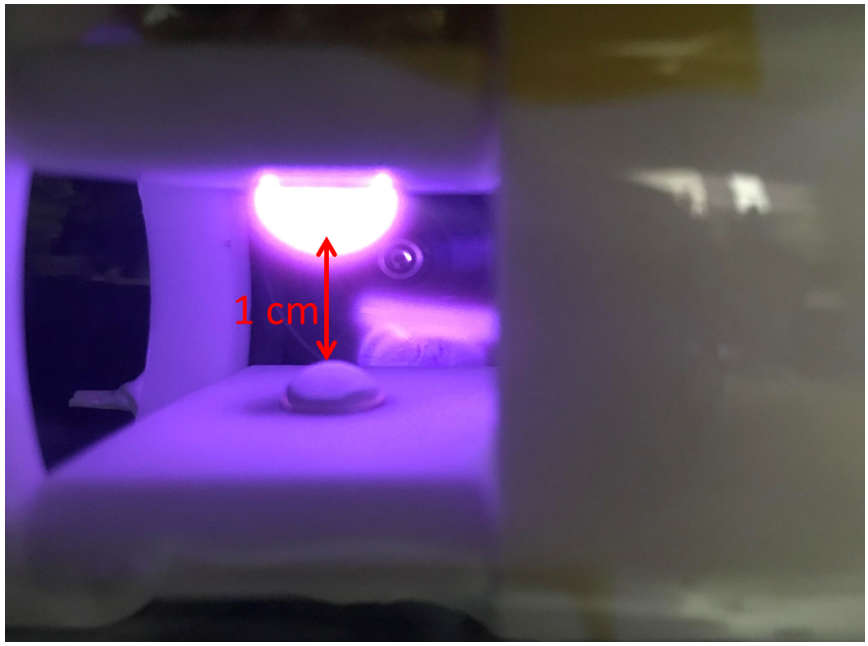

Figure 3.12: DC argon plasma during Langmuir probe test.

The upper electrode in the image is the anode (+) and the lower electrode is the cathode (-). The plasma is concentrated on the anode, extending only 2-3 mm from the rivet. Sheath formation around the Langmuir probe causes it to glow as well. The probe could not be adjusted to contact the main body of the plasma due to the plasma's small size. If the probe came into contact with the ionizing electrode, the source meter would have been destroyed.

The lack of immersion in the plasma resulted in an uncharacteristic IV curve. Typically, ion saturation current is close to zero, dwarfed in magnitude by electron saturation current. With this plasma, we see the opposite. An IV curve from this plasma is displayed in Figure 3.13.

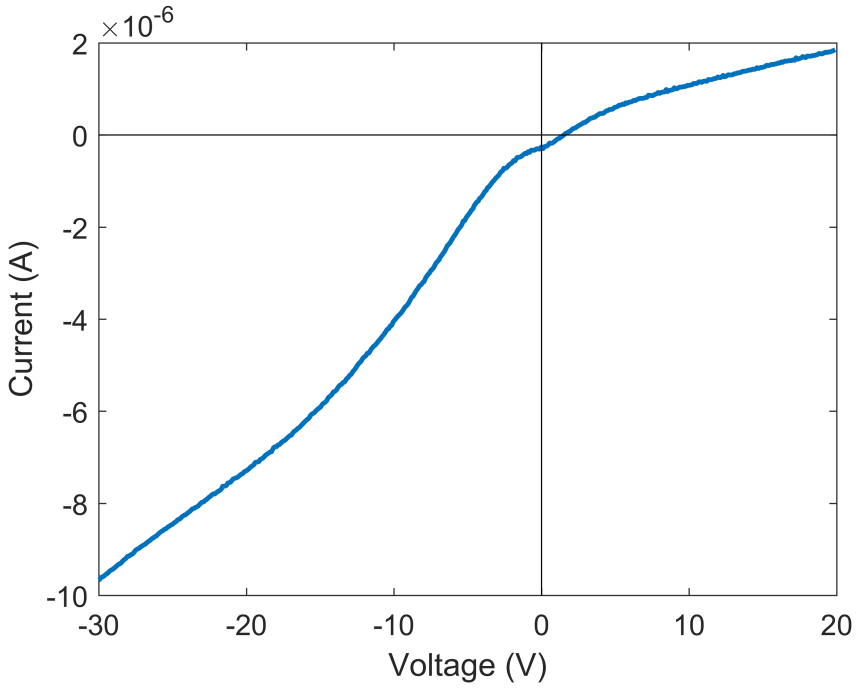

Figure 3.13: IV Curve from 450 V DC plasma Langmuir probe test.

This plasma's uncharacteristic curve does not yield to the OML analysis method. The test bed would need to be redesigned to support probe tests with full immersion in the plasma for reliable results with DC ionization.

3.3.2 DC Spectrometer Measurements

Spectra from the plasma was measured at a variety of ionization voltages. A plasma from the highest recorded test voltage (450 V) is analyzed here. For DC spectra measurements, 20 scans were taken and averaged. The integration time of each scan was 300 milliseconds.

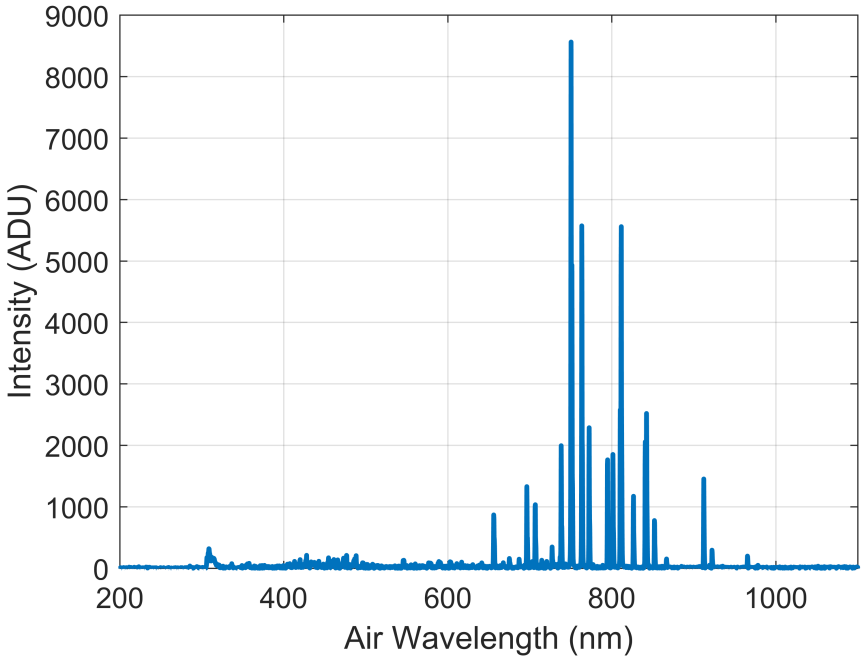

Figure 3.14: Measured spectra from 450 V DC, 1 Torr argon plasma.

In argon, the neutral lines (Ar I) are concentrated around 800 nm, while the singly-ionized lines are in the 400 nm range. Figure 3.14 shows that for this case, the most intense lines are generated by neutral argon, which is clearly the dominant species. Experimental line ratios are simply calculated from the peak intensity of the selected lines. Parameter determinations via the line ratio method will be discussed in Chapter 4.

3.4 Nanosecond Pulsed Plasma Measurements

3.4.1 Langmuir Probe

Langmuir probe measurements are typically performed on plasma columns that have reached a steady state. The pulsed plasma does not reach steady-state at the nanosecond ionization speeds: it is either ionizing or de-ionizing. Complex triggering systems can be designed to support time-resolved probe measurements. Langmuir probe tests can be performed on pulsed plasma and provide an approximation of the plasma's parameters [19]. The pulsed

DC supply generated a large enough volume of plasma to at least partially immerse the probe, evident in Figure 3.15.

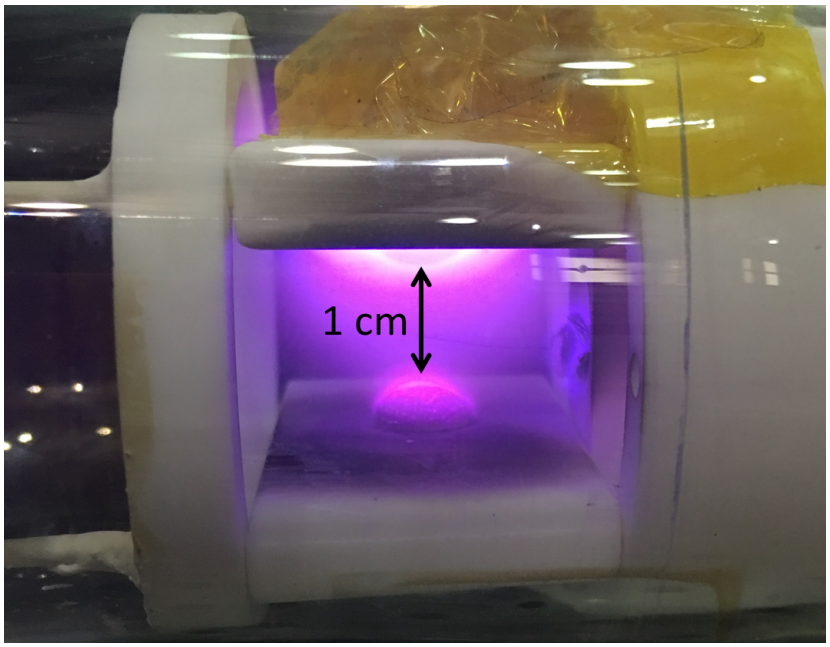

Figure 3.15: Plasma generated at 1 Torr with 1 kV, 5 ns pulses.

The measured IV curve has an ion saturation current magnitude comparable to its electron current magnitude. This is not the ideal IV curve shape, but applying OML methods yields curves and parameter values one would expect from a steady-state Maxwellian plasma. The curve in Figure 3.16 was initially hidden by current spikes, likely caused by arcing in the plasma. The major current spikes were removed prior to analysis, but some are still apparent. The processed curve is displayed in Figure 3.17.

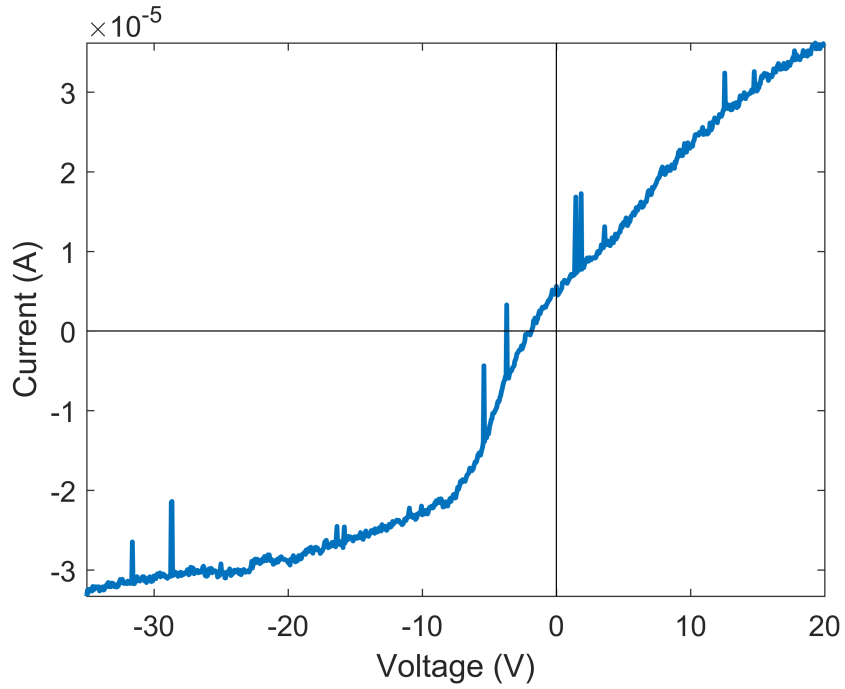

Figure 3.16: Pulsed plasma IV curve.

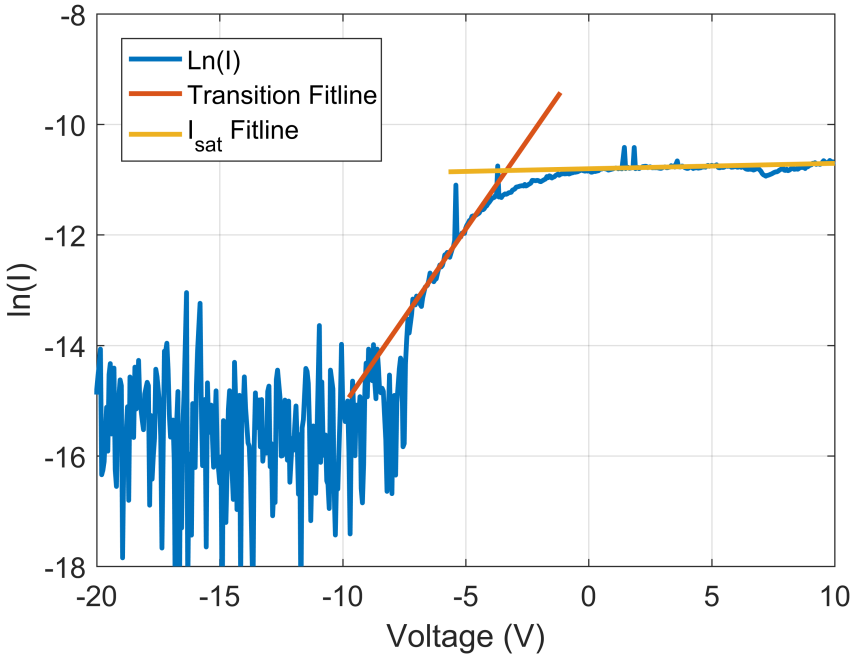

Figure 3.17: Processed IV curve using OML technique.

Using the fit lines with the OML equations, the electron temperature is calculated to be

1.558 eV and the electron density is calculated to be 2.88×10^{13} /m^3. While these measured values are close to the order of expected values, they should be approached with caution. The effects of transients like ionization and de-ionization on Langmuir probe measurements are not well defined. These probes are susceptible to plasma sheath effects, which may play a role in the morphology of the measured IV curve. Additionally, the fit lines used to analyze the data affect the calculated values. Finally, the probe tip surface area's inclusion in the electron density calculation adds more uncertainty. The total surface area was used in the calculations, but a partial immersion would cause the calculated value to be lower than the actual value.

3.4.2 Pulsed Spectrometer Measurements

The plasma analyzed here was generated by the FID pulsed voltage with 1 kV, 5 ns long pulses at a pulse repetition frequency of 50 kHz. Because the spectrometer's minimum integration time is 30 ms long, it captures many pulses of light during each scan. The integration time on the spectrometer is set to 150 ms for these tests to make the weak ion lines stand out. This results in the averaged spectra of approximately 7500 pulses per scan. 20 scans are taken and averaged for each test. The results from this measurement are displayed in Figure 3.18.

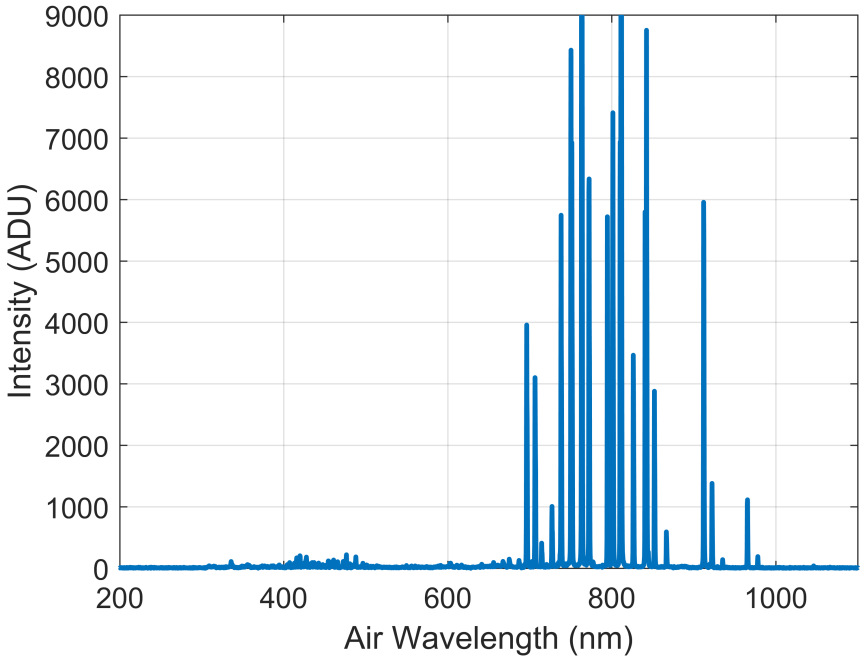

Figure 3.18: Measured spectra from 5 ns, 1 kV pulsed, 1 Torr argon plasma.

Similar to the DC plasma test, the strong lines are concentrated around 800 nm, meaning that Ar I is the predominant species. As the plasma is ionized and de-ionized, it emits light at wavelengths corresponding to its properties at each point in its lifetime. Thus, single pulse emits light at a variety of spectra. While measuring the spectra at each point in time would be ideal for determining the evolution of its properties, this is no easy task and would require a much more sophisticated set of equipment than what was used. The spectra measurements represent the average spectra over the plasma's lifetime. Here, it is assumed that the average optical spectra represent the plasma's average parameters over a single pulse. The average parameters will be applied to light curve data. Line ratio calculations using this measured data will also be applied in Chapter 4.

CHAPTER 4
COLLISIONAL RADIATIVE MODEL

In this chapter, we will utilize a theoretical model to infer the plasma properties (namely electron temperature and density) based on the measurements presented in Chapter 3. These properties can be inferred through analysis of the intensity of light emitted from the plasma at individual wavelengths. The intensity of light at each of the wavelengths is a function of gas density and the degree of ionization in the plasma. The peak intensity of one line can be divided by another, yielding a 'line ratio.' Line ratios vary with the degree of ionization as well. Line ratios are calculated for experimental plasmas and compared to models to determine experimental plasma parameters. Radiative models take a plasma's background gas and other experimental parameters into account to generate theoretical spectra, calculating electron density concurrently. Experimental line ratio is compared to that of a number of theoretical plasmas to determine the experimental plasma's parameters. PrismSPECT is a commercially available radiative model used to synthesize spectra, which will be used to apply the line ratio method for conductivity calculations.

4.1 PrismSpect Simulations

PrismSPECT generates emission simulations of a variety of gases and mixture ratios. The background gas pressure, plasma geometry, and electron temperatures can all be varied in testing. At the simplest level, a radiative model like PrismSPECT determines the density of each excited state for a plasma of a given level of ionization and gas density. The intensity of light emitted at a given wavelength is directly correlated to the population density of the particle's corresponding excited level [13]. Low pressure (10^{-2} Torr) plasmas can be modeled with the Corona model, which takes into account only electron impact excitation and radiation from excited electrons. For a plasma at our test pressures, the more compli-

cated collisional radiative model (CRM) is more appropriate. CRMs account for processes within the plasma such as electron impact excitation from both ground and metastable levels, spontaneous radiation and radiation trapping, and chamber wall interactions [14]. These processes occur frequently in higher-pressure plasmas and affect the densities of excited states in a plasma, and therefore the plasma's radiated spectra. These processes, along with electron temperature and gas density, are plugged into a set of rate balance equations used to determine the steady-state density of each species (Ar I, Ar II, etc.) in a plasma. The density of each excited state is directly correlated to the intensity of light at that state's corresponding wavelength. Model spectra is calculated from the state densities.

PrismSPECT includes a variety of spectra modeling modes, but low-temperature spectroscopy will be used here. The other modes prove useful for 'hot' plasmas seen in fusion reactor experiments such as the ones in [20]. The gas temperature is set to the ambient temperature of the testing, approximately 300 K. The plasma geometry is set to zero-width for simplicity and simulation speed. For the line ratio method, pressure will be fixed and electron temperature will be varied in the non-LTE simulation mode. When a simulation is complete, the spectra and ionization information from each simulation is available, along with individual line intensity information. Changes in electron temperature are apparent in the spectra, shown below in Figure 4.1. The dominant lines in the 1 eV plasma are neutral Ar I lines around 800 nm. As electron temperature is increased, the singly ionized Ar II lines grow in intensity around 400 nm. The increase in intensity of the Ar II lines is indicative of an increase in singly ionized species. To observe the effect of electron temperature on the species present in the plasma, PrismSPECT tracks the fraction of the plasma's mean charge resulting from each species as shown in Figure 4.2. As the plasma's electron temperature is increased, more higher order species are ionized, resulting in an increase in electron density, which is calculated by the software. Figure 4.3 shows electron density as a function of electron temperature. By comparing simulated spectra to measured spectra, the corresponding electron temperature and electron density can be found and used to calculate

the plasma's conductivity.

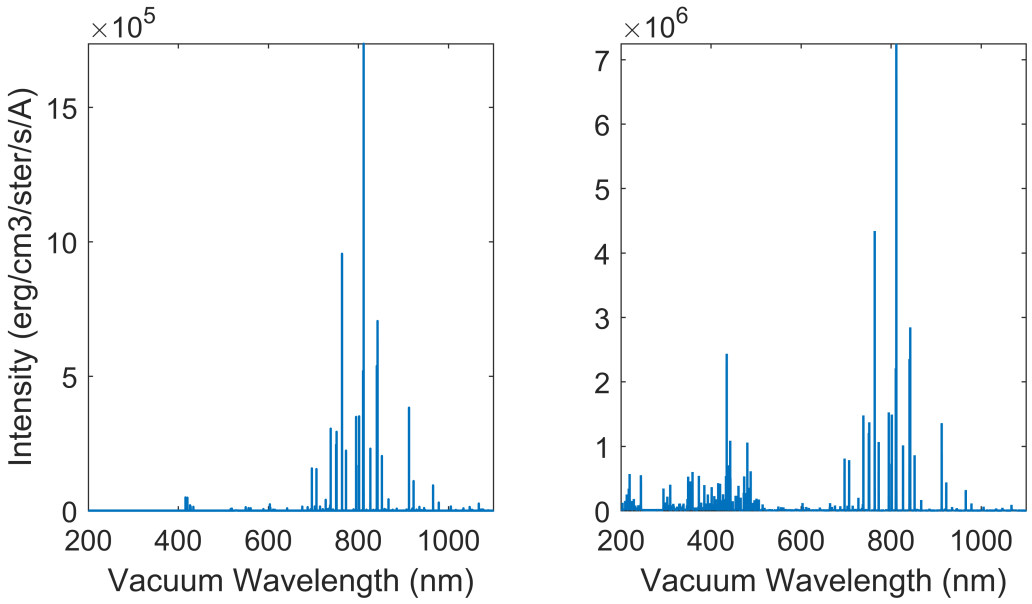

Figure 4.1: Optical emissions of 1 eV (left) and 1.5 eV (right) from argon plasma at 1 Torr (PrismSPECT simulation).

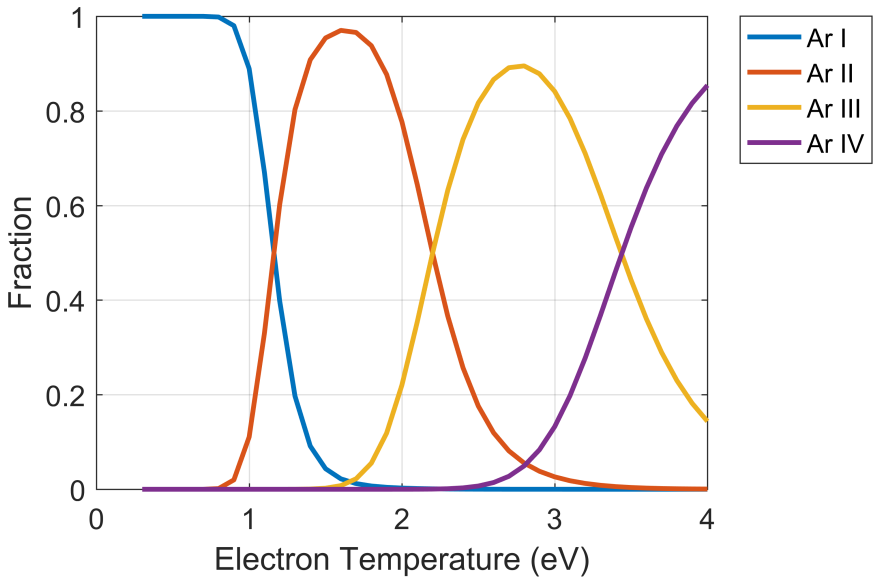

Figure 4.2: Mean charge fraction of species vs. electron temperature at for argon plasma at 1 Torr (PrismSPECT simulation).

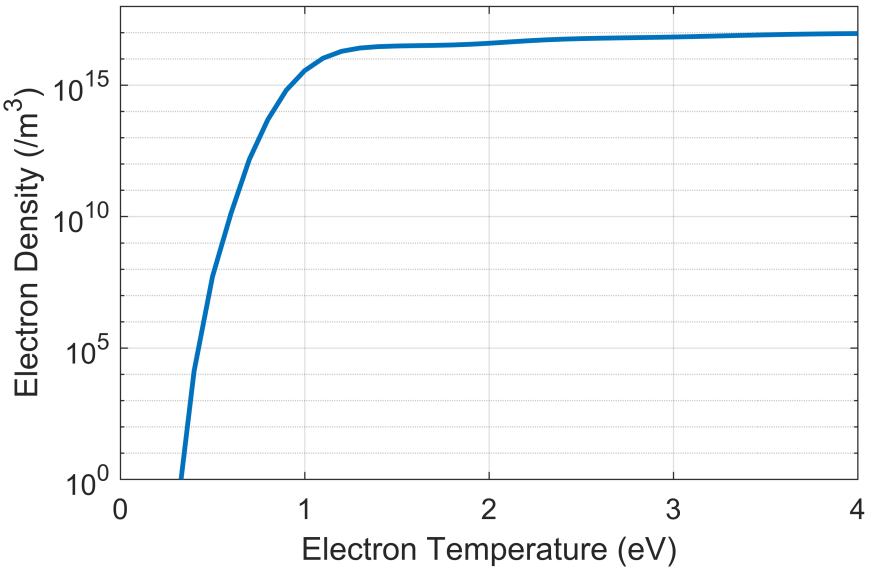

Figure 4.3: Electron density vs. electron temperature for argon plasma at 1 Torr (PrismSPECT simulation).

4.2 Line Ratio Method

PrismSPECT's built-in line intensity viewer tracks the optical emission resulting from a given transition as plasma simulation parameters are varied. The ratio of one line intensity trace to another yields the plasma's line ratio as a function of electron temperature. To determine the electron transitions generating the plasma's optical emissions, measured emission data was compared to the NIST atomic database [21]. The database displays the know photon wavelengths generated from a given element when ionized. Examination of argon's lines presented an issue: many of the observed wavelengths with strong lines fall within a nanometer of another strong line. The Ocean Optics HR4000 spectrometer used for measurements has a wavelength resolution of 0.75 nm FWHM. A spectrometer's limited wavelength resolution can cause peak overlap, obscuring the intensity measurement of multiple lines by recording them as a single line with a summed intensity. This effect is problematic for the line ratio method, which relies on peak values of individual lines. The

list of candidate lines was narrowed down by selecting only isolated lines (2 nm away from other lines) in the NIST data. Neutral (Ar I) and singly ionized (Ar II) lines were detected. A comparison of line intensities between the two species is a good indicator of the plasma's degree of ionization, so three lines of each species is chosen for comparison to simulated line ratios. The chosen wavelengths are listed below in Table 4.1.

Table 4.1: Detected isolated lines of Argon plasma.

Energy Level	Vacuum Wavelength (nm)	Photon Energy (eV)
Ar I	738.6014	1.6787
Ar I	763.7208	1.6234
Ar I	912.2967	1.3586
Ar II	454.6326	2.7271
Ar II	465.9205	2.6610
Ar II	476.4864	2.6013

Figure 4.4 shows the evolution of two line intensities as electron temperature is varied, and Figure 4.5 shows the evolution of the ratio of the two selected lines. To determine the electron temperature of the experimental plasma, its line ratio for a given pair of lines is calculated and matched to the simulated data. Multiple ratios will be tracked, and their resulting electron temperatures and densities will be averaged.

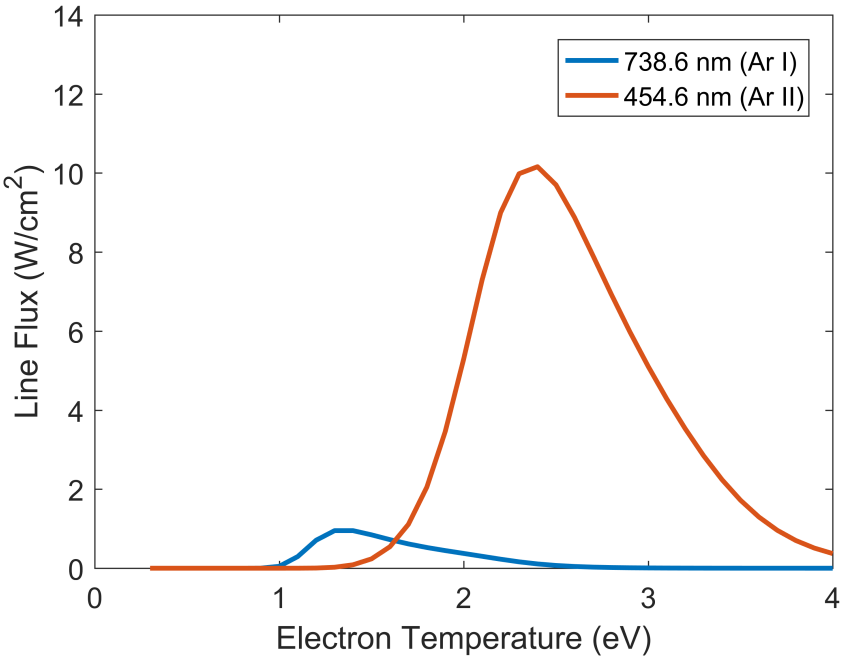

Figure 4.4: Argon line intensities vs. electron temperature.

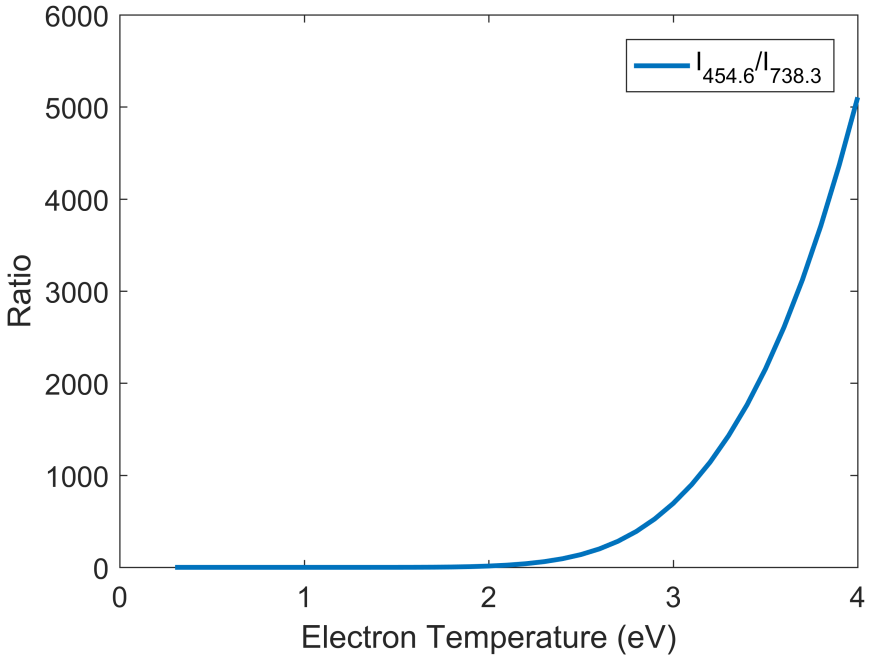

Figure 4.5: Line ratio of Ar II line (454.6 nm) to Ar I line (738.6 nm) vs. electron temperature.

4.2.1 DC Plasma Line Ratio

In PrismSpect, a zero-width, non-LTE style simulation is run at the test pressure and temperature, sweeping through electron temperatures. The peak intensity of the selected lines is tracked, and the line ratios are calculated as a function of electron temperature. Two PrismSpect simulations are run when calculating line ratios to account for computational limitations. The first simulation covers a wide range of electron temperatures at a relatively low resolution (0.1 eV). The second simulation covers the range of electron temperatures determined by the first test at a higher resolution (0.01 eV). For the 450 V test, PrismSPECT's line ratio simulations indicate an electron temperature between 1.49 and 1.56 eV with a standard deviation of 0.031 eV. This low variation is a good indication of PrismSPECT's consistency in line ratio calculations. The mean electron temperature is 1.5211 eV, and the average electron density is 3.099×10^{16} /m^3. Figures 4.6, 4.7, and 4.8 display the experimental line ratios for each pair of line intensities plotted against the PrismSPECT simulation results. Experimental line ratios are displayed as dashed lines, while the simulation-generated line ratios are the solid curves.

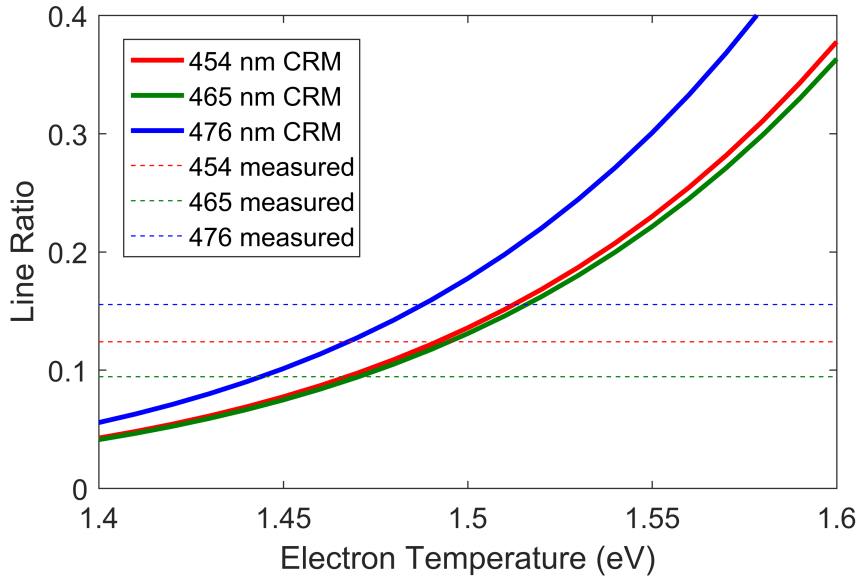

Figure 4.6: Ratios of Ar II line intensities to 738.3 nm Ar I line intensity, experimental DC plasma comparison.

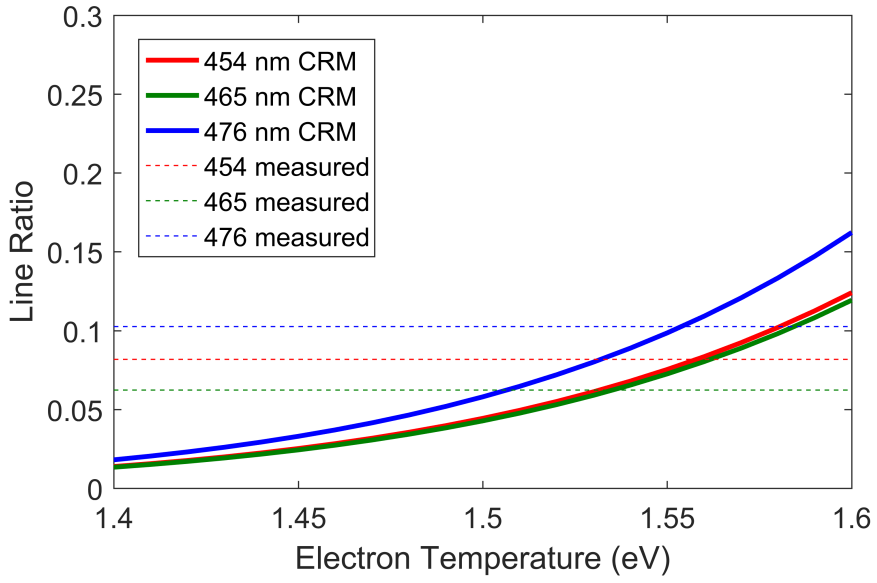

Figure 4.7: Ratios of Ar II line intensities to 763.5 nm Ar I line intensity, experimental DC plasma comparison.

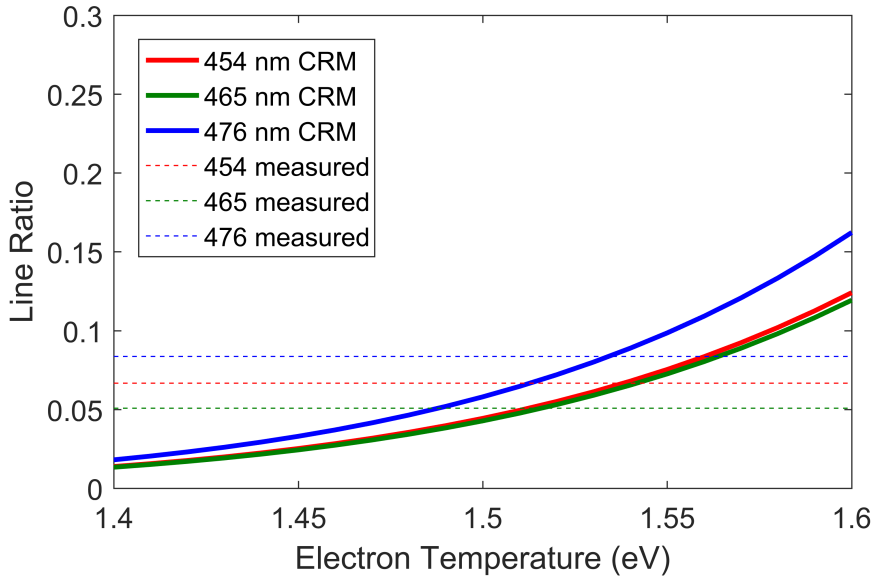

Figure 4.8: Ratios of Ar II line intensities to 912.2 nm Ar I line intensity, experimental DC plasma comparison.

4.2.2 Nanosecond Pulsed Plasma Line Ratio

The 763.5 nm line used in the DC analysis section was not present in the pulsed plasma spectra analyzed below. For this test, PrismSPECT's line ratio simulations indicate an electron temperature between 1.27 and 1.35 eV with a standard deviation of 0.0341 eV. The variation here is comparable to that in the DC measurements. The mean electron temperature is 1.31 eV, and the average electron density is 2.6179×10^{16} /m^3. Figures 4.9 and 4.10 display the experimental line ratios.

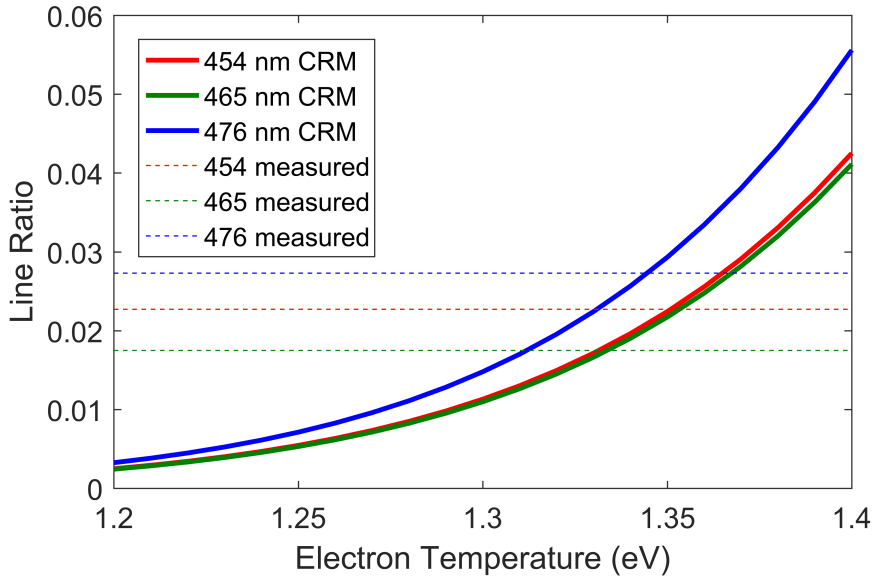

Figure 4.9: Ratios of Ar II line intensities to 738.3 nm Ar I line intensity, 5 ns pulsed DC plasma comparison.

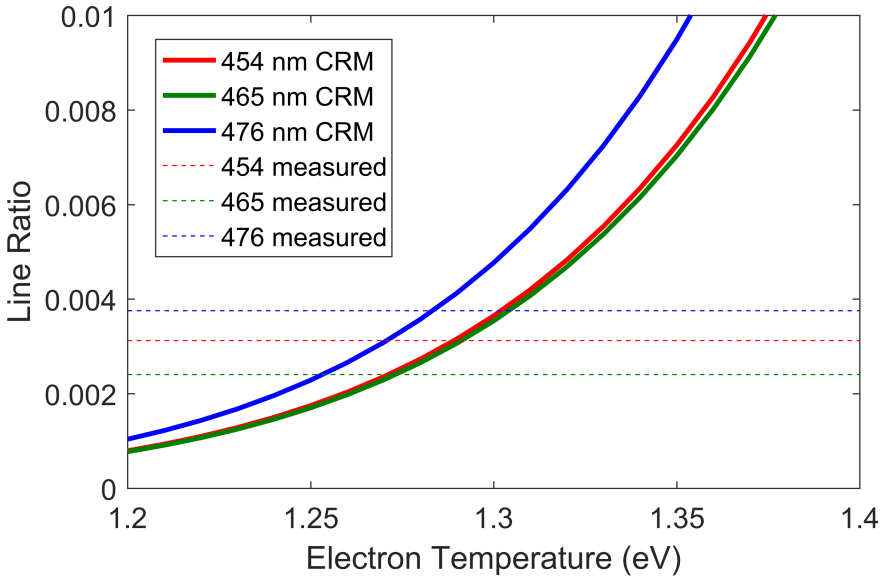

Figure 4.10: Ratios of Ar II line intensities to 912.2 nm Ar I line intensity, 5 ns pulsed plasma comparison.

CHAPTER 5

ATTENUATION SIMULATIONS FOR EXPERIMENTAL PLASMA

In this chapter, the attenuation model described in Chapter 2 is applied using the experimentally-inferred properties measured in Chapter 4. For a DC plasma, this is a straightforward application, but for an AC or pulsed plasma, the plasma's transient nature must be taken into account. As before, the pulse length is the length of time an input pulse's voltage is greater than zero, with the Gaussian standard deviation set equal to one-eighth of the pulse's duration.

5.1 DC Plasma Attenuation

The resistance function for a 1 cm radius plasma column is calculated using the line ratio parameter calculations and is shown on the left Figure 5.1. This plasma has a resistance of 1534 Ω/m for frequencies well below the plasma frequency. This resistance is too high for use as a conductor if the length is any appreciable fraction of a meter (our goal is an antenna on the order of meters long). To decrease resistance while keeping the plasma parameters fixed, the plasma column's radius may need to be increased. Increasing the plasma's radius to 10 cm would decrease the resistance by a factor of 10, but this would also require an ionizing voltage that is 10 times higher, so practical considerations may preclude this approach. Nonetheless, we will discuss the larger 10-cm plasma in our analysis here. The resistance function is calculated for a 10 cm radius plasma column and is shown on the right in Figure 5.1, with a resistance of 15.3 Ω/m in the low-frequency region. The larger plasma will be used for analysis to show the effects of the ramp-up in resistance near the plasma frequency. Increasing the plasma's electron density would also lower the resistance in the low-frequency regions. However, this increase would change the plasma frequency. Fixing the plasma frequency allows the examination of the plasma's ability to

conduct a pulse's high-frequency content. Figure 5.2 shows pulse attenuation in a 10 cm radius plasma column with the experimental plasma's parameters. A 5 ns long pulse and a 1 ns long pulse are modeled. The 5 ns long pulse (left) is attenuated by a factor of 65% as it travels a distance of 3 meters through the experimental plasma. The 1 ns long pulse (right) is attenuated by a factor of 96% over the same distance.

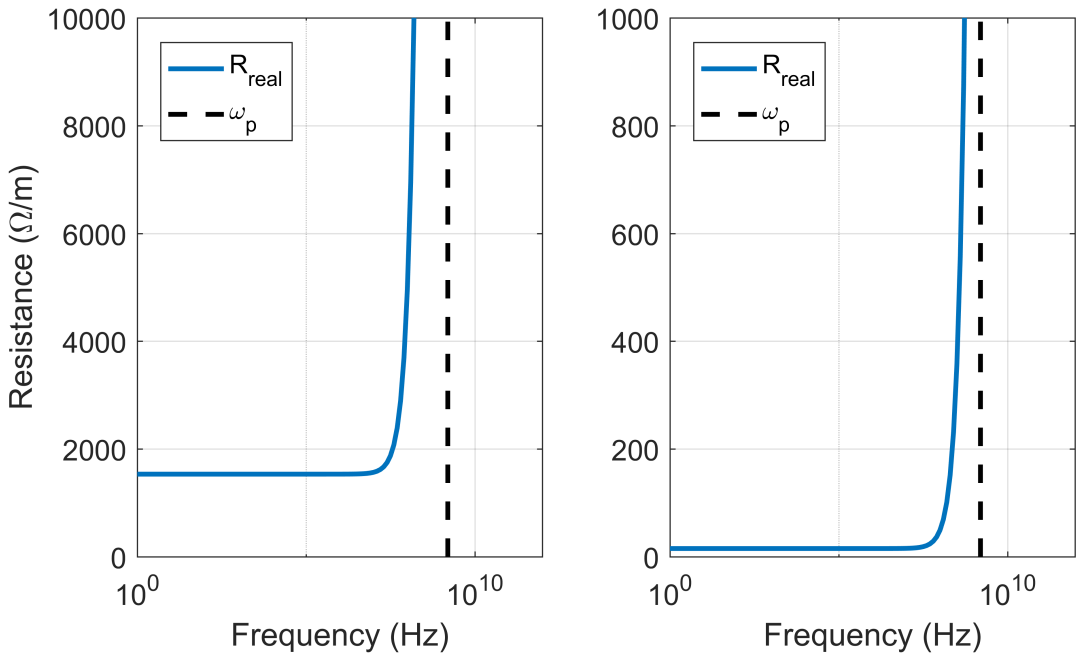

Figure 5.1: Resistance of experimental DC plasma column with 1 cm radius (left) and 10 cm radius (right) vs. frequency.

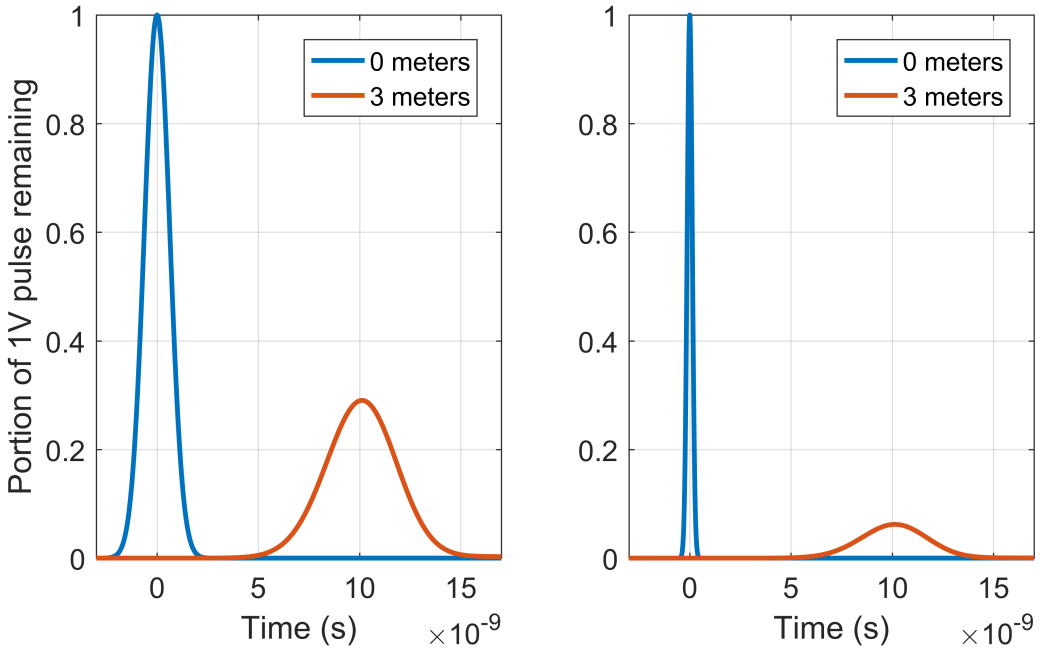

Figure 5.2: 5 ns pulse (left) and 1 ns pulse (right) attenuation in 10 cm radius, 3 meter long plasma column with measured DC argon plasma properties.

Unfortunately, the plasma's electron density is too low to support lossless propagation at either of these pulse repetition frequencies. Methods to improve electron density will be discussed in Chapter 6.

5.2 Pulsed Plasma Attenuation

The parameters calculated for the pulsed plasma can then be applied to a light curve to infer the plasma column's conductivity as a function of time. The light curves from the photodetector are wavelength-integrated power measurements as a function of time. The photodetector's output voltage scales approximately linearly with total light detected over its operating wavelength range, so they are useful in a relative sense even though these measurements are not absolutely calibrated. To compare this data to simulations, ratios of the values in the curve are taken relative to its average, shown in Figure 5.3.

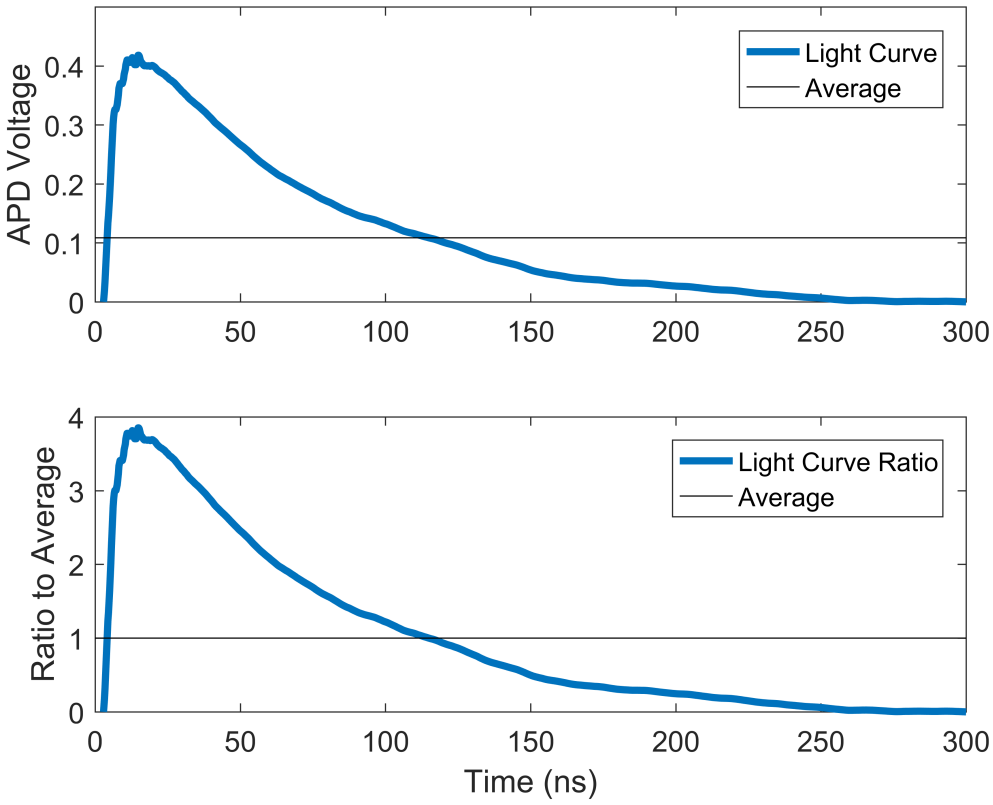

Figure 5.3: Light curve (upper) and light curve ratio-to-average (lower).

To determine conductivity as a function of time, the plasma's parameters calculated via the line ratio method are applied to the light curve. For this analysis, it is assumed that the spectra produced by the plasma at the measured electron temperature is indicative of the plasma's average light output. While this assumption is imperfect, it allows the development of an analysis technique that can be applied when time-resolved line intensity measurements are taken. A plasma's total optical output does not scale linearly with electron temperature. PrismSPECT's line intensity tool can calculate wavelength-integrated light output as a function of electron temperature. The spectra is integrated over the photodetector's wavelength operating range (200-1000 nm). The intensities are converted to ratios corresponding to the intensity at the measured electron temperature, 1.31 eV. CRM-calculated intensity and intensity ratio plots are shown in Figure 5.4.

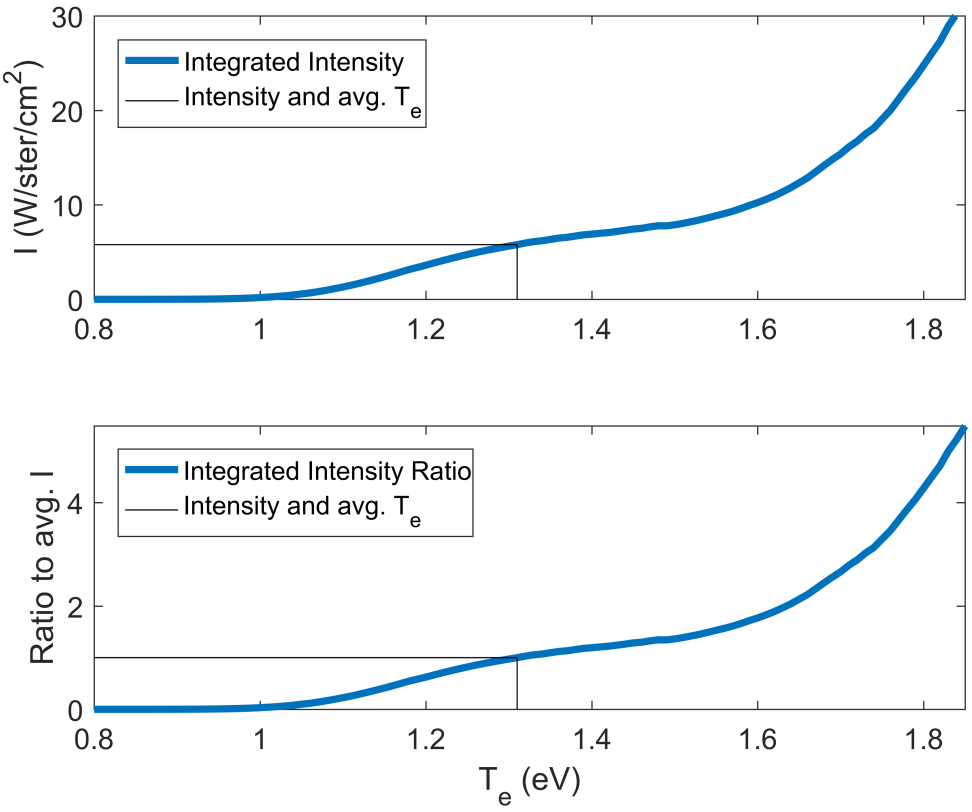

Figure 5.4: Integrated intensity vs. T_e (upper); Integrated intensity ratio-to-average vs. T_e (lower).

The CRM-calculated intensity ratios are compared to the light curve ratios to determine the plasma's electron temperature and density evolution in time, plotted in Figure 5.5.

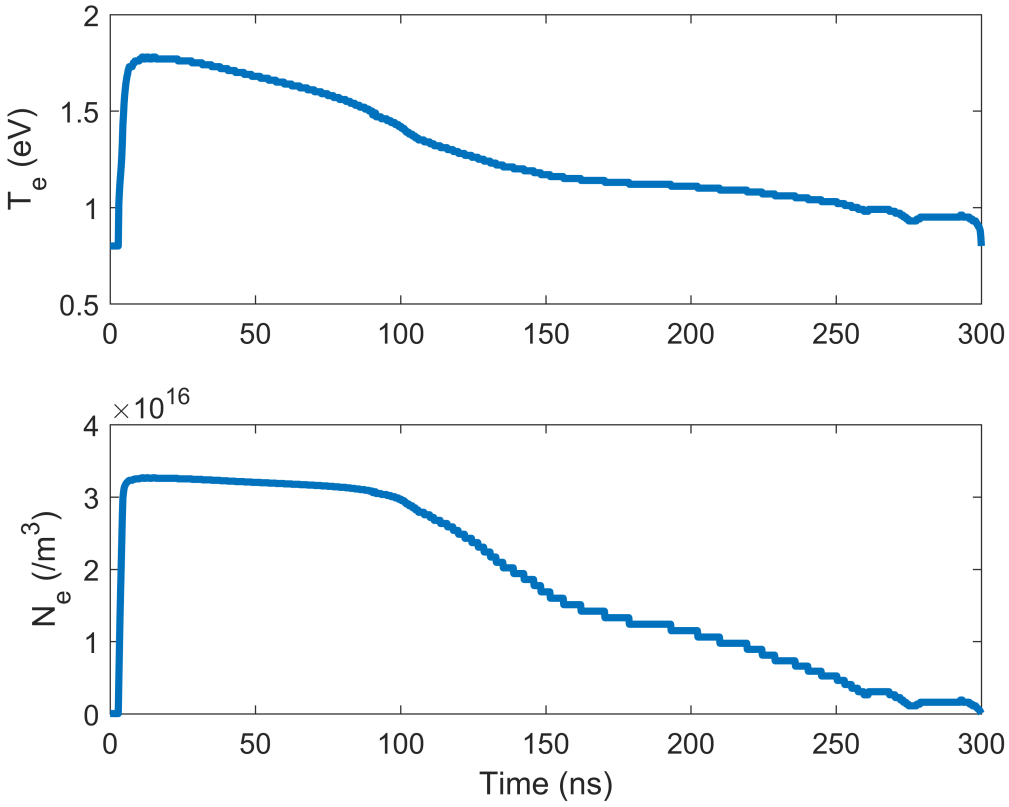

Figure 5.5: Plasma electron temperature vs time (upper); electron density evolution in time (lower).

The plasma's conductivity and ability to conduct a pulse of a given width changes in time according to these parameters. By running the pulse attenuation code with these changing parameters at a variety of pulse repetition frequencies, the upper limit on pulse length becomes apparent. Figure 5.6 shows this plasma's pulse attenuation evolution, with the cross sectional radius set to 10 cm.

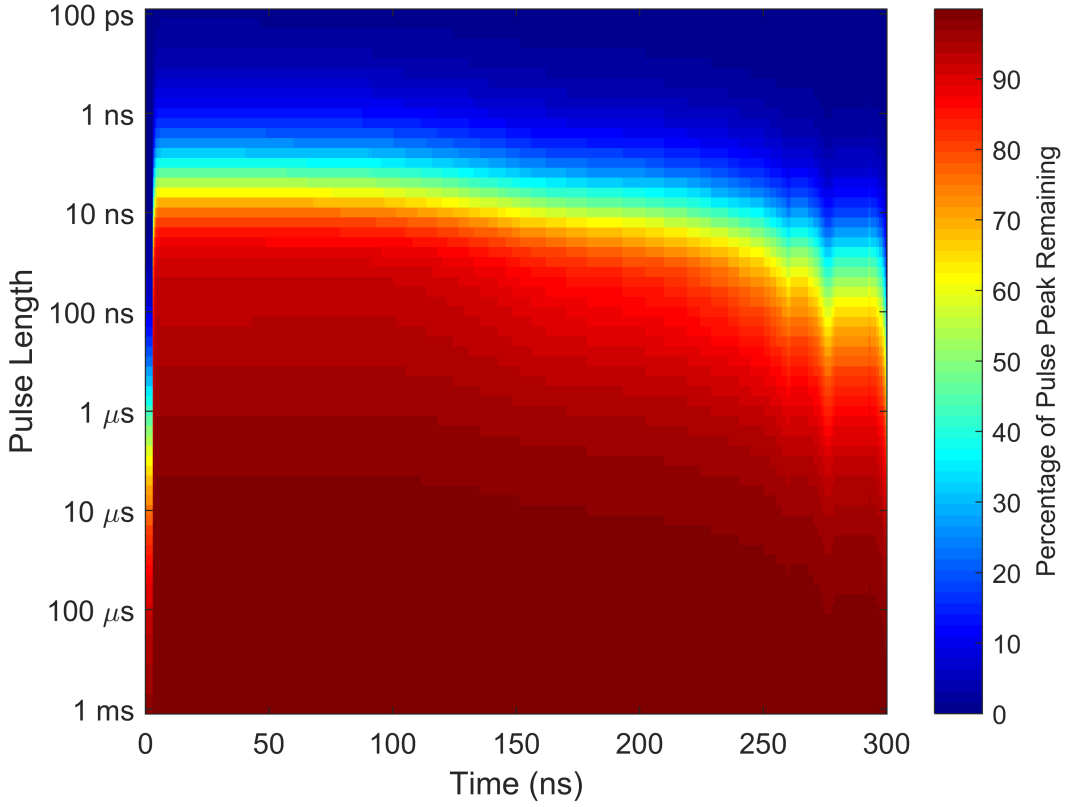

Figure 5.6: Voltage pulse attenuation in time-varying plasma at various pulse lengths.

The shortest pulse this plasma can sustain without loss is 10 μs long. With speed of light propagation, a pulse of this time would be approximately 3 km long in space. For the reflection suppression concept to be realized, pulses need to be less than 10 ns long.

CHAPTER 6
CONCLUSION

6.1 Summary

In this thesis, we were able to implement optical analysis techniques to determine the electromagnetic properties of nanosecond pulsed plasma. Measured parameters were utilized in a basic propagation model to determine the viability of test plasma columns as conductors for the time-domain matching technique. Benchmarks have been set for future research: electron density needs to be pushed to the order of 10^{18} or higher, and de-ionization time needs to be decreased considerably. While the plasma columns generated in this research did not reach quality benchmarks, the analysis methods developed will be applied to future research as the experimental design is improved.

6.2 Future Work

6.2.1 Increasing Pressure

The plasma generated with the current experimental configuration does not have a high enough electron density or fast enough quench time to support the desired pulse lengths. Future work should focus on methods to increase electron density and speed up quenching. Simulations with the pulse loss model show that the plasma's electron density needs to be on the order of 10^{18} or higher to support nanosecond timescale voltage pulse propagation. Increasing the test pressure in the plasma chamber may increase electron density. To determine a target test pressure for future experimentation, we turn to PrismSPECT, running simulations at a variety of pressures and electron temperatures. The result is the heat map style plot in Figure 6.1. The vertical axis is simulation pressure in Torr while the horizontal axis is electron temperature. We estimate the that the desired density can be

obtained at pressures as low as 50 Torr when ionized to electron temperatures near 1.5 eV. Atmospheric pressure (760 Torr) can yield desired densities around 1.2 eV. While higher pressure plasma don not need to be ionized as strongly as lower pressure plasmas, they are much harder to generate. Setting the gap size to 1 cm, the Paschen curve predicts a 1.5 kV breakdown voltage at 50 Torr. At atmospheric pressure, breakdown voltage is approximately 15 kV. Applied voltage would need to be higher than breakdown voltage to obtain the highly-ionized plasmas necessary for high electron densities. Furthermore, ionization pulse reflections cause breakdown to occur at voltages higher than the Paschen threshold when pressure is increased. This inefficiency must be overcome with higher amplitude voltage pulses. Higher pressures also result in a faster de-ionization time, which is beneficial for the pulsed antenna concept.

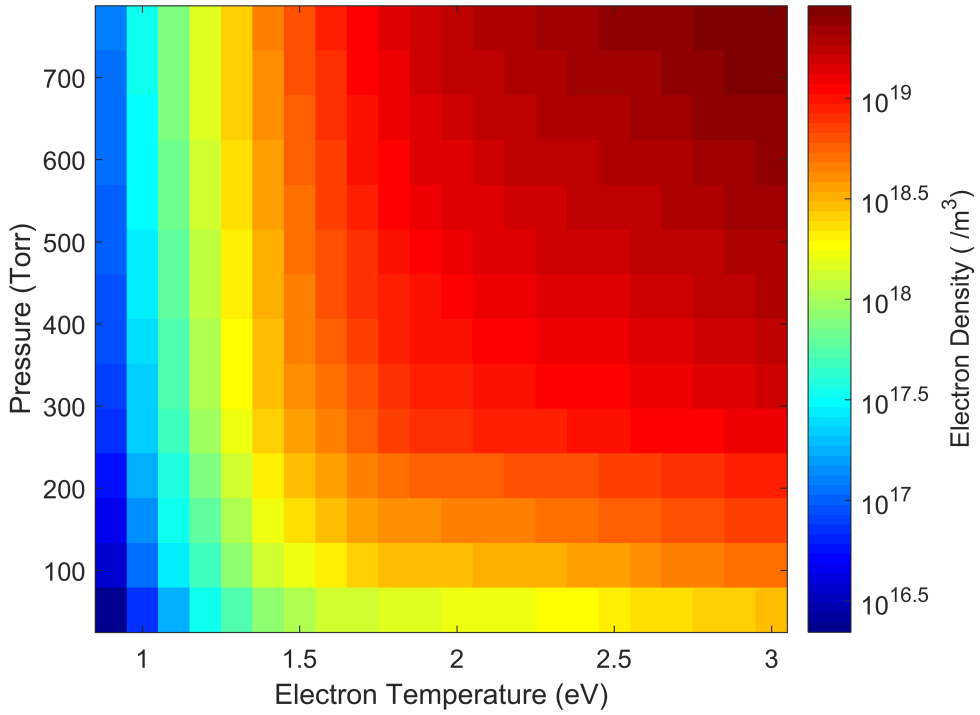

Figure 6.1: Electron density as a function of chamber pressure and electron density from PrismSPECT data.

6.2.2 High Speed Photometric Line Tracking

To properly apply the line ratio method as a time evolution analysis technique, individual line intensities need to be tracked in time. The high-conductivity portion of the plasma pulse is likely shorter than what is shown in the simulation output from Chapter 5. The spectrometer's integrating action over time hides time-varying light output characteristics important to a fully-developed model. Individual lines can be tracked using a monochromator and photomultiplier tube as in [20]. A monochromator is an optical device that is used to mechanically isolate a narrow band of wavelengths. Individual line intensities were tracked with 10 nanosecond resolution in the plot in Figure 6.2. The horizontal axis is time, and the vertical axis is photocurrent, which is proportional to line intensity.

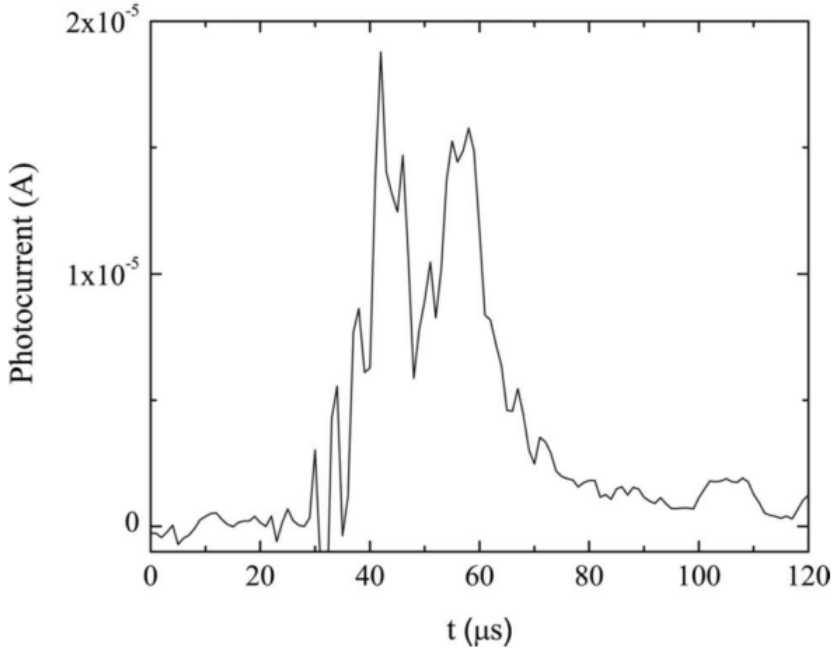

Figure 6.2: C III 97.7 nm line from Spheromak experiments [20].

A time-resolved line ratio can be calculated by tracking multiple lines through monochromator testing. Applying PrismSPECT to the data will allow an accurate time-resolved conductivity calculation.

REFERENCES

[1] A. Watt, *VLF Radio Engineering: International Series of Monographs in Electromagnetic Waves*, Volum 14. Pergamon Press, 1967, ISBN: 1483119882.

[2] L. A. Thompson, "Broadband Electrically Short Transmitters Via Time-Varying Antenna Properties," PhD thesis, Georgia Institute of Technology, 2017.

[3] U. Inan and M. Gołkowski, *Principles of plasma physics for engineers and scientists*. 2010, vol. 9780521193, pp. 1–270, ISBN: 9780511761621.

[4] F. Paschen, "Ueber die zum Funkenübergang in Luft, Wasserstoff und Kohlensäure bei verschiedenen Drucken erforderliche Potentialdifferenz," *Annalen der Physik*, vol. 273, no. 5, pp. 69–96, 1889.

[5] R. Massarczyk, P. Chu, C. Dugger, S. R. Elliott, K. Rielage, and W. Xu, "Paschen's law studies in cold gases," *Journal of Instrumentation*, vol. 12, no. 6, 2017.

[6] T. Anderson, *Plasma Antennas*. Norwood, MA, 2011, pp. 13–30.

[7] I. Alexeff, T. Anderson, S. Parameswaran, E. P. Pradeep, J. Hulloli, and P. Hulloli, "Experimental and theoretical results with plasma antennas," *IEEE Transactions on Plasma Science*, vol. 34, no. 2 I, pp. 166–172, 2006.

[8] D. C. Jenn, "Plasma Antennas: Survey of Techniques and the Current State of the Art," Naval Postgraduate School, Tech. Rep., 2003.

[9] N. S. J. Braithwaite, "Introduction to Gas Discharges," *Plasma Sources Science and Technology*, vol. 9, no. 4, pp. 517–527, 2000.

[10] I. Dildar, S Rehman, M Khaleeq-ur Rahman, and K. Bhatti, "Collective behavior of silver plasma during pulsed laser ablation," *Laser Physics*, vol. 25, no. 7, pp. 76–102, 2015.

[11] F. F. Chen, "Langmuir Probe Diagnostics," in *Mini-Course on Plasma Diagnostics, IEEE-ICOPS meeting, Jeju, Korea, June 5, 2003*, 2003, pp. 1–40.

[12] *Plasma Diagnostics - Plasma Characterisation Using a Langmuir Probe by Hiden Analytical*, 2008.

[13] U Fantz, "Basics of plasma spectroscopy," *Plasma Sources Science and Technology*, vol. 15, S137–S147, 2006.

[14] X.-M. Zhu and Y.-K. Pu, "Optical emission spectroscopy in low-temperature plasmas containing argon and nitrogen: determination of the electron temperature and density by the line-ratio method," *Journal of Physics D: Applied Physics*, 2010.

[15] D. Pozar, *Microwave Engineering*, 3rd ed. Hoboken, NJ: Wiley, 2005.

[16] U. S. Inan and A. S. Inan, *Engineering Electromagnetics*. Menlo Park: Addison Wesley Longman, Inc., 1999, pp. 1–804.

[17] C. Chan, "Experimental Investigation of Fast Plasma Production for the VAIPER Antenna," Master's Thesis, Georgia Institute of Technology, 2017.

[18] W. Bowls, "The Effect of Cathode Material on the Second Townsend Coefficient for Ionization by Collision in Pure and Contaminated N2 Gas," *Physical Review*, vol. 53, pp. 293–300, 1937.

[19] S. J. Doyle, K. E. Evdokimov, A Brockhaus, C Borchardt, and J Engemann, "Langmuir probe measurements in commercial plasma plants," *Plasma Sources Sci.Technol*, vol. 3, pp. 539–544, 1994.

[20] V. H. Chaplin, M. R. Brown, D. H. Cohen, T. Gray, and C. D. Cothran, "Spectroscopic measurements of temperature and plasma impurity concentration during magnetic reconnection at the Swarthmore Spheromak Experiment," *Physics of Plasmas*, 2009.

[21] *NIST Atomic Spectra Database*.